Turbulent Mixing in Stratified Fluids – Layer Formation and Energetics

By

Young-Gyu Park

B.S., Seoul National University, Seoul, Korea, 1987
M.S., Seoul National University, Seoul, Korea, 1989

Submitted in partial fulfillment of the
requirements for the degree of

Master of Science in Oceanography

at the

MASSACHUSETTS INSTITUTE OF TECHNOLOGY

and the

WOODS HOLE OCEANOGRAPHIC INSTITUTION

September 1993

Signature of Author _____
Joint Program in Oceanography
Massachusetts Institute of Technology
Woods Hole Oceanographic Institution

Certified by _____
Dr. John A. Whitehead
Thesis Supervisor

Accepted by _____
Dr. Lawrence J. Pratt
Chairman, Joint Committee for Physical Oceanography
Massachusetts Institute of Technology
Woods Hole Oceanographic Institution

Turbulent Mixing in Stratified Fluids - Layer Formation and Energetics

By

Young-Gyu Park

Submitted in partial fulfillment of the requirements for the degree of
Master of Science in Oceanography
at the Massachusetts Institute of Technology
and the Woods Hole Oceanographic Institution

September 1993

Abstract

A turbulent mixing experiment was conducted to observe the dynamics and the energetics of layer formation along with the region of layer formation in the Reynolds number (Re) and the overall Richardson number (Ri_o) space. A salt stratified fluid was mixed uniformly throughout its depth with a vertical rod that moved horizontally at a constant speed. The evolution of density was measured with a conductivity probe.

As the instability theory of Phillips (1972) and Posmentier (1977) shows, an initially uniform density profile turns into a series of steps when Ri_o is larger than a critical value Ri_c, which forms a stability boundary. For fixed Re, as Ri_o decreases to Ri_c, the steps get weaker; the density difference across the interface and the difference of density gradient between layers and interfaces become small. Ri_c increases as Re increases with a functional relation $log\, Ri_c \approx Re/900$. The steps evolve over time, with small steps forming first, and larger steps appearing later through merging and decay of the interfaces. After some time the interior seems to reach an equilibrium state and the evolution of the interior steps stops. The length scale of the equilibrium step, l_s, is a linear function of U/N_i, where U is the speed of the rod and N_i is the buoyancy frequency of the initial profile. The functional relationship is $l_s = 2.6U/N_i + 1.0cm$. For $Ri_o < Ri_c$, the mixing efficiency, R_f, monotonically decreases to the end of a run. However, for $Ri_o > Ri_c$, the evolution of R_f is closely related to the evolution of the density field. R_f changes rapidly during the initiation of the steps. For $Ri_o \gg Ri_c$, R_f increases initially, while for $Ri_o \gtrsim Ri_c$, R_f ecreases initially. When the interior reaches an equilibrium state, R_f becomes uniform. Posmentier (1977) theorized that when steps reach an equilibrium state, a density flux is independent of the density gradient. The present experiments show a uniform density flux in the layered interior irrespective of the density structure, and this strongly supports the theory of Posmentier. The density flux generated in the bottom boundary mixed layer goes through the interior all the way to the top boundary mixed layer without changing the interior density

structure. Thus, turbulence can transport scalar properties further than the characteristic length scale of active eddies without changing a density structure. When the fluid becomes two mixed layers, the relation between R_f and Ri_l was found for $Ri_l > 1$. Here, Ri_l is the local Richardson number based on the thickness of the interface. R_f does decrease as Ri_l increases, which is the most crucial assumption of the instability theory.

Thesis Supervisor:
Dr. John A. Whitehead, Senior Scientist
Woods Hole Oceanographic Institution

Acknowledgments

Thank Dr. Jack Whitehead. He is more than an advisor and his guidance and encouragement made this thesis possible.

Karl Helfrich also encouraged and helped me to set up the equipment. Glenn Flierl guided me kindly. Comments from Ray Schmitt and Rui Xin Huang were useful.

Anand Gnanadesikan and Jack Whitehead gave me the initial idea of this work and discussion with Anand was helpful. I cannot forget friendship from Joe LaCasce, who is my only classmate, and Bob Frazel in GFD lab. Bob also helped me during the experiment. Abbie Jackson in Education Office teaches me English.

I also thank Korean Government who gave me a chance to study in US.

It is dedicated to my parents in Korea.

Contents

Chapter 1

Introduction

After the invention of rapid response themistors, ocean observations have shown the widespread occurrence of microstructure in the density field. On occasion, a microstructure is in the form of a succession of layers and interfaces. The density is almost uniform in each layer and jumps nearly discontinuously across the interfaces that separate the layers. Since the direct measurement of any vertical flux is as yet technically difficult, the scalar microstructure has been used to estimate the turbulent vertical fluxes of some scalar quantities such as heat, salt, and density. But the energetics, i.e., the conversion of turbulent kinetic energy to mean potential energy, of turbulent mixing in stratified fluids is poorly understood and the estimation of the vertical fluxes is based on models, which do not include the dynamics of microstructure.

So far, most laboratory turbulent mixing experiments have focused on the bulk transport across interfaces (Turner , 1968, Linden, 1979, 1980). In those experiments, two mixed layers with a sharp density interface between them were prepared in a suitable tank. Turbulence was then introduced in one or both layers and the evolution of the density in each layer was measured. The mixing efficiency, R_f, was parameterized using external parameters such as the Reynolds number, Re, and the Richardson number, Ri, which is the ratio between potential energy stored in stratification and available kinetic energy. The experiments show that as Ri increases from zero, R_f also increases from zero to a maximum, and then decreases as Ri becomes even larger.

These experiments have been useful in determining the mixing properties of stratified fluids with fully developed layers, but they may not be appropriate for describing the mixing properties when layers start to develop from a uniformly stratified state.

Those experiments also cannot answer under what conditions microstructure occurs. Phillips (1972) and Posmentier (1977) developed theories for microstructure formation. A statically stable uniform stratification may be unstable to turbulence so that turbulence breaks down a uniform stratification to another structure, a series of layers and interfaces. The most important assumption of the theories is the relation between R_f and Ri. As Ri increases from zero to a critical Richardson number Ri_c, R_f increases from zero to a maximum. If Ri increases further beyond Ri_c, R_f decreases as shown Figure 1-1a. If Ri of the initial state is larger than Ri_c, turbulent mixing amplifies perturbations in a density field accompanying a change in a density flux or mixing efficiency. The density structure stabilizes while evolving to a succession of steps.

There are a few laboratory turbulent mixing experiments focused on layer formation. Ivey and Corcos (1982), and Thorpe (1982) stirred linearly stratified fluid with vertical grids moving laterally. A series of turbulent mixed layers intruded into the non-turbulent ambient fluid away from the grid so that a step-like structure was generated at the outside of the active turbulent region. Thorpe (1982) tried to relate the step-like structure to the local instability theory of Phillips/Posmentier, but he could not verify the theory. Ivey and Corcos (1982) showed that the intrusive layer was due to the collapse turbulent eddies in stratified surroundings and the intrusion made a negligible direct contribution to vertical buoyancy flux so that the intrusive layers could not satisfy one of the necessary conditions of the theory.

Ruddick, McDougal and Turner (1989, RMT afterward) stirred salt or sugar stratified fluids horizontally with an array of vertical rods throughout the depth and length of a tank. The initial linear stratification evolved into a series of steps when the stirring was weak and the steps disappeared as the stirring became strong as the theory of Phillips/Posmentier predicted. Until now, RMT is the only experiment that examines Phillips/Posmentier's theory. But RMT was an exploratory experiment and

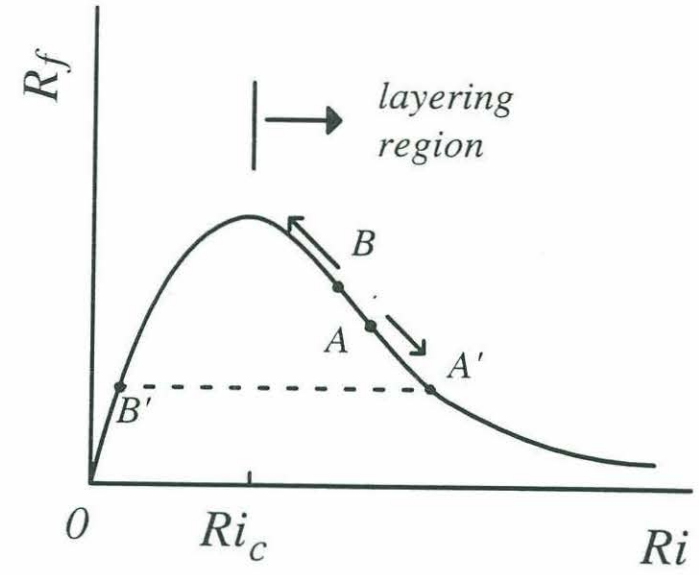

(a)

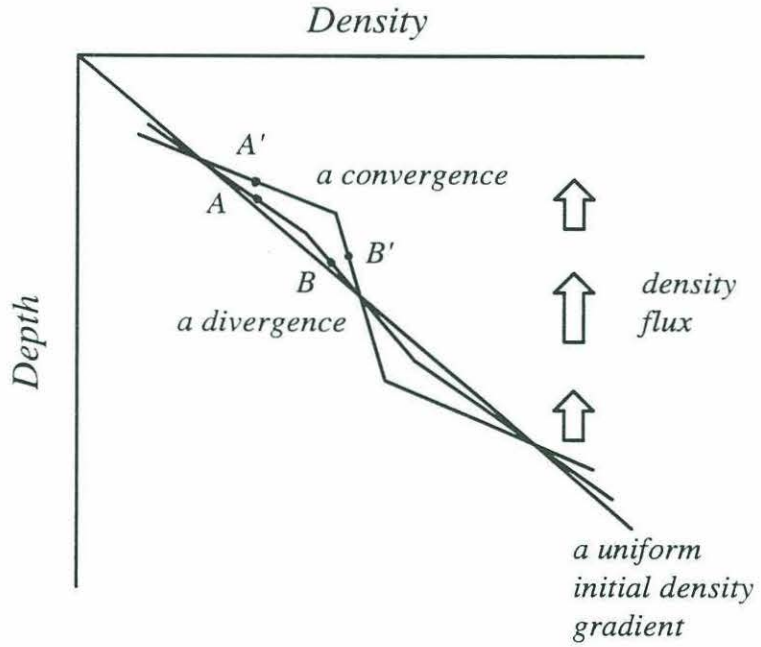

(b)

Figure 1-1: (a) The relation between the mixing efficiency, R_f, and the suitably defined Richardson number Ri. Layering is expected to the right of the point Ri_c, where R_f is maximum. (b) A schematic diagram of the evolution of density profile when $Ri_o > Ri_c$. At the point A, Ri increases and a convergence of buoyancy flux occurs. At the point B, Ri decreases and a divergence occurs. The perturbation intensifies until the buoyancy flux across each point becomes the same.

many questions remain unanswered. Among them the most fundamental questions are "*What does the stability boundary look like*, in other words, *what is the relationship between* Ri_c *and* Re*?*", and "*What are the energetics of layer formation?*".

In the present experiments, an almost linearly salt stratified fluid was stirred uniformly with a rod at constant speed until the fluid was completely mixed. The evolution of the density profile was measured with a conductivity probe that has a resolution of about one millimeter. A linear motion system was used to control the mixer and the probe so that it was possible to get accurate control of the rod speed and estimate potential energy changes of the density field. The energy budget was used to investigate the energetics of layering, focusing on the difference between the layering and non-layering cases. Since the fluid was mixed until it became almost homogeneous, it was possible to relate the mixing efficiency and density flux to the evolution of the density field. Finally, by changing the stratification and the Reynolds number as widely as the apparatus allowed, the stability boundary for layer formation was found.

In Chapter 2, the theoretical background is discussed. The chapter also contains the design and procedure of the experiments. In Chapter 3, the evolution of the density profiles depending on the parameters of the experiments is described, focused on the evolution of layers and interfaces. The stability boundary is also discussed in this chapter. In Chapter 4, the length scale of the steps is discussed related to the external parameters of the experiments. The energetics of the layer formation are also discussed related to the evolution of the density structure. Chapter 5 contains conclusions and suggestion for further studies.

Chapter 2

Theoretical Background and the Experiments

2.1 Theoretical Background

Phillips (1972) and Posmentier (1977) proposed similar hydrodynamic instability theories for microstructure formation. Far away from boundaries, in the presence of turbulence, a linear density profile may be unstable to small perturbations in the vertical density gradient, if the stratification is strong enough or the turbulence is weak enough.

The theory is based on the relation between the flux Richardson number, R_f, and a suitably defined Richardson number, Ri. They assume that R_f increases from zero to the maximum as Ri increases from zero to a critical Richardson number, Ri_c. In addition, R_f decreases as Ri increases beyond Ri_c as in Figure 1-1a. Physically, if $Ri > Ri_c$ then turbulence is suppressed and turbulence cannot mix a density field effectively. If $Ri < Ri_c$ then turbulence is active, but there is not much density difference to mix so that turbulence cannot mix the density field efficiently. If Ri has an intermediate value, a density field is most efficiently mixed. Now, assume that initially there is a homogeneous turbulence and a constant turbulent vertical buoyancy flux throughout a uniform density gradient. Let the vertical density gradient be perturbed locally as illustrated in Figure 1-1b. Ri is increased where the vertical

density gradient is intensified (point A), and decreased where the density gradient is weakened (point B). R_f changes in response to the change of Ri. If the initial Ri is larger than Ri_c then the positive part of the perturbation decreases the buoyancy flux while the negative part of the perturbation increases the buoyancy flux locally. Thus, a divergence of the buoyancy flux happens where the density gradient is weakened, and a convergence happens where the density gradient is intensified. The perturbation intensifies further until the point B moves to the left along the curve to the point B', and the point A to the right to the point A'. The buoyancy flux across the layers and interface are balanced so that a *steady state* or *an equilibrium state* is achieved. Posmentier (1977) showed that in the steady state, the buoyancy flux becomes a constant irrespective of density gradient. However, his theory cannot determine the constant.

In contrast to the above situation, if $Ri < Ri_c$ initially, then the positive part of a perturbation in the density field causes a divergence in the density flux, and the negative part of a perturbation causes a convergence. Therefore, the perturbation cannot grow, but decays. In their papers, Phillips uses the relation between a buoyancy flux and a vertical density gradient, and Posmentier uses a salt flux and the gradient of a salt, instead of R_f and Ri. But R_f and Ri are equivalent to a density flux and a density gradient, respectively. Posmentier calculated the evolution of the vertical salinity distribution numerically with an empirical relation between vertical eddy diffusivity, K, and Ri. Both Phillips and Posmentier explained the instability of strong stratification under turbulence, but they could not predict the length scale of a layer. Basically, their equations are diffusion equations with negative diffusion coefficients or time reversed diffusion equations, so the smallest scale grows most rapidly, which is very unlikely in a real situation. Phillips suggested that the minimum length scale in nature should depend on the smallest scale over which the buoyancy flux can be regarded as a local function. Posmentier pointed out that scales larger than the scale of turbulence are meaningful.

The most critical assumption of Phillips/Posmentier's theory is the dependence of the flux Richardson number, R_f, on the Richardson number, Ri. There are many

experiments that have tried to find the relation between R_f and a suitably defined Richardson number. Those experiments are usually called turbulent entrainment experiments (Turner, 1968, Linden, 1979, 1980). Two mixed layers of fluid are prepared and then turbulence is introduced to either upper or lower layer. The changes in the density of each layer are measured so that the relationship between R_f and Ri is constructed. Turner (1968) shows the decrease of the mixing efficiency as the Richardson number increases. The rate of the decrease depends on the scalar quantity used, but it clearly decreases. With this result, the whole trend can be indirectly inferred, since R_f should approach zero as the Richardson number decreases to zero. Linden (1979) combined previous experimental results with his own experiment to show this trend. Due to the difference between the mechanical mixers, each data set showed different maximum mixing efficiency. By dropping a horizontal grid across a density interface, Linden (1980) shows the whole trend. Recently, Ivey and Imberger (1991) produced the relationship using an energetic argument along with the results of the existing grid generated turbulent mixing experiments. To scale the data, the overturn Froude number was used instead of the Richardson number. The overturn Froude number is the square root of the inverse of the Richardson number based on turbulent length and velocity scales. The results verify the relation between R_f and Ri.

2.2 The Experiments

2.2.1 The design of the experiment

The objective of the experiments is to create turbulence by stirring a linearly stratified fluid with a rod, and to observe the evolution of the density field after numerous stirring events. To characterize the energetics, it is necessary to calculate the energy input and the change in potential energy accurately. To meet these requirements, a conductivity probe was used to get density profiles of high spatial resolution. A linear motion system connected to programmable drivers was used to control the speed of the stirring rod.

The most important parameters of the experiments are the Reynolds number of the rod, Re, and the overall Richardson number, Ri_o. The definitions are

$$Re = \frac{UD}{\nu},$$

$$Ri_o = \frac{N_i^2 D^2}{U^2}.$$

Here, N_i, is the buoyancy frequency of an initial stratification, U the speed of the rod, ν kinematic viscosity, and D the diameter of the rod. Other parameters are the Péclet number, $Pe = UD/\kappa_s$, and the Prandtl number, $Pr = \nu/\kappa_s$, where κ_s is the molecular diffusivity of salt. Only salt was used in preparing stratified fluids so that Pr was fixed throughout the experiments, and Pe was effectively the same as Re.

2.2.2 Apparatus and procedure

Using the Öster method, an almost linearly salt stratified fluid was filled into a $20cm \times 10cm \times 45cm$ Plexiglas tank. The initial stratification was measured with a conductivity probe at the beginning of every run. A vertical rod of diameter D was used as a stirrer with D being either $1.29cm$, $2.26cm$ or $3.33cm$. The tip of the rod was placed $0.5cm$ above the bottom of the tank. The rod was connected to a sliding carriage driven by a stepper motor by means of a threaded rod. The stepper motor driver was controlled by a computer so that precise driving speeds could be obtained. The rod moved back and forth a programmed distance at constant speed throughout each run. One back and forth motion was defined as an *excursion*, and the length of one excursion was $28cm$ in all runs. The speed of the rod varied between 1 and $7cm/sec$. After repeating the excursion a predetermined number of times, the stirring rod was stopped for one or two minutes while energetic turbulence decayed. This was confirmed visually using a shadowgraph during some runs. Then, the conductivity probe was lowered by another stepper motor. A *cycle* that consisted of a sequence of stirring, waiting and profiling was repeated until the fluid was almost mixed. A

schematic diagram of the experiment is shown in Figure 2-1.

Since the conductivity data was used to get the density structure, calibration of the probe was important. The probe is a model 125 four-prong (two active and two passive) conductivity microprobe made by Precision Measurement Engineering. The probe has an effective sampling volume of $1mm^3$ and a time constant in the range of $10^{-3}second$ or faster. It was calibrated before each run with five samples of water. The density of the samples was measured directly with a densiometer (Anton Paar model DMA 46) precise to $10^{-4}g/cm^3$. The probe was never taken out of the water throughout a run. The tip of the probe moved from $0.5cm$ below the water surface to about $1cm$ above the bottom at a speed of $1cm/sec$. During the downward motion it was stopped at about every millimeter to measure the conductivity, which was stored in the computer for later use. A shadowgraph was also used to observe turbulence. Time lapse movies and still pictures were taken during some runs. The screen for the shadowgraph was placed either at the wall or about $1m$ in front of the tank to produce optimally focused images.

Since a temperature change could also cause some mixing, the temperature of the laboratory was kept constant. When a run took more than a day, the room temperature was recorded with a thermometer placed next to the tank. The variation of the room temperature was less than $2°C$ over a day. To avoid mixing due to the temperature difference between the laboratory and the test fluid, the fluid was placed in the laboratory more than 12 hours before the filling. At the time of filling the temperature difference between the room and the fluid was less than $1°C$. Sideways heating can form layers of depth scale $l_t = \alpha\Delta T/(\partial\rho/\partial z)$. Here, α is the thermal expansion coefficient, ΔT is the temperature difference between the fluid and the room, and ρ is density. In the present experiments, l_t was less than $1cm$, which was smaller than the diameter of the smallest rod used. The tank was constructed of $3/8inch$ thick Plexiglas to retard lateral heat transfer so that the effect of the temperature variation should not be significant.

The experiments were divided into two phases. The first phase focused on making steps with turbulent mixing, and observing the evolution of a density profile. RMT

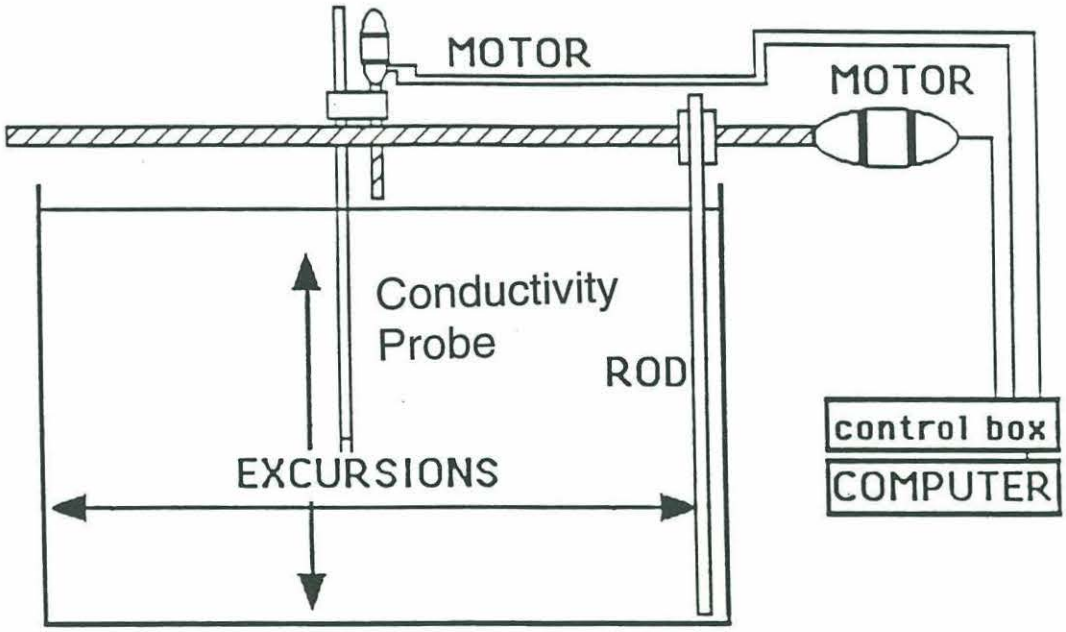

Figure 2-1: The schematic diagram of the experiment

found that layering occurred when stratification was strong and stirring was weak. Several different stratifications were tested within a narrow range of Re variation. The present experiments showed layers when the stratification was strong as RMT showed. Three different sizes of the rods were used to see if the sizes of the rods changed the step size.

The second phase was focused on finding a stability boundary between the layering and non-layering cases. Wide ranges of Re and Ri_o variations were produced within the limits of the apparatus. The change of Ri_o was obtained by changing both the stratification and the speed of the rod. The change of Re was obtained by varying the speed of the rod while D, the size of the rod, was fixed at $2.26cm$.

The parameters of all the 75 runs are listed in Appendix 1, and every run is plotted in the (Re, Ri_o) space as illustrated in Figure 2-2. Re was varied from around 100 to 1600 and Ri_o from 0.2 to 12.3. Since keeping Re constant is easier than preparing the same stratification for each run, the runs are aligned along a constant Re line in the (Re, Ri_o) phase space.

2.2.3 Data Correction

The conductivity profile was converted to a density profile using the reading from the five samples of water with the density known to $10^{-4}g/cm^3$. The raw density profile was processed before any calculations were made, although it showed trends or characteristics clearly. First, density was extrapolated to top $5mm$ and bottom $1cm$ where the conductivity was not measured. Second, sometimes the probe generated noise spontaneously. This happened in the later stages of some runs. The data was smoothed by applying 9 point moving average. Third, the linear drift of the probe was corrected using mass conservation. The total mass of the fluid should be conserved during a run, if the effect of evaporation is neglected. The evaporation was at most less than $1mm/day$. The evaporation caused less than 5% changes of the mean density throughout a run, and all the density profiles of a run were shifted to give the same mean density. The conductivity probe is very sensitive to temperature change. During a run, the room temperature changed less than $2°C$ over a day, and

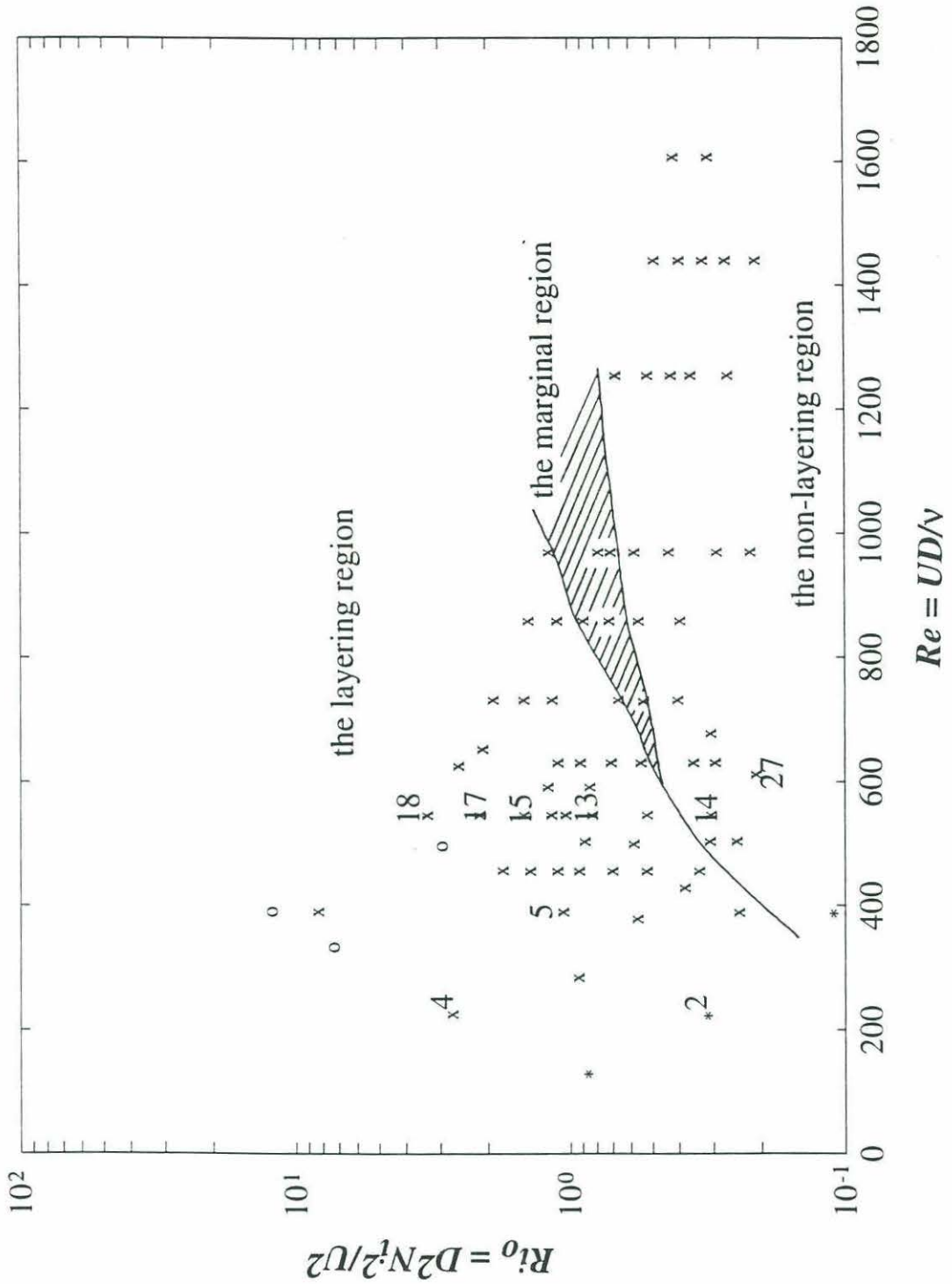

Figure 2-2: The stability curve and all the 75 runs in the (Re, Ri_o) space. Here, * is for 1.29cm diameter rod, x for 2.26cm rod, and o for 3.33cm rod. In the figure, the hatched region denotes a marginal region. The region above the hatched region is an unstable region (the layering region) and below is a stable region (the non- layering region). The boundary between the marginal region and the layering region is the stability boundary. The numbers in the figure denote runs shown in the following figures.

the effect of the temperature variation was neglected. The corrected data set was used in the potential energy calculation.

Chapter 3

Observations

3.1 The evolution of the density profile

Every run exhibited the development of mixed layers at the top and bottom of the tank before significant variations happened to the interior density field. The condition of zero flux across the horizontal boundaries requires vanishing vertical density gradient so that boundary mixed layers are produced. These boundary mixed layers are independent of the layer produced in the interior, which is the focus of this study. Initially the thicknesses of the boundary mixed layers are less than the turbulent region, which is the same as the depth of the tank. The boundary mixed layers expand into the stratified interior with time due to the no flux condition at the horizontal boundaries. Thus the expansion of the boundary mixed layer does not require an increase in the turbulent region or an increase in the strength of turbulence. The structure of the boundary mixed layers is basically the same in every case. The density gradient was close to zero and varied smoothly. However, the interior showed different patterns of evolution depending on the external parameters such as Re and Ri_o.

For fixed Re, the evolution of the interior density structure is described for different values of Ri_o. For small Ri_o, the density profile shows two boundary mixed layers and the interior of almost constant density gradient. The transition from the boundary layers to the interior is smooth. No intensification of density gradient is observed as

shown in Figure 3-1a. Re and Ri_o of this run (Run 14) are 547 and 0.31, respectively. The interior density gradient looks like a wide plateau in each profile with small scale "wiggles" of about $1.3cm$ as shown in Figure 3-1b. The wiggles are present from the beginning to the end of the run. They were observed in many cases regardless of the external parameters but did not become amplified in any case. They were presumably due to turbulent fluctuations. Since the wiggle length scale is never amplified in any runs, the presence of these small wiggles is henceforth neglected when explaining the structure of the interior. As time progresses, the height of the plateau decreases very slowly. The width also decreases monotonically due to the expansion of the boundary layers. Figure 3-2 is a series of shadowgraphs taken during Run 14. The black vertical strip is the stirring rod of diameter being $2.26cm$. No interface can be found.

For a run with larger Ri_o, interfaces form first between the interior and boundary mixed layers as shown in Figures 3-3a and 3-3b. Re and Ri_o of this run (Run 13) are 547 and 1.04, respectively. The density gradient shows a clear difference from the preceding density gradient, which is Figure 3-1b, but the density profile only seems slightly different when Figures 3-1a and 3-3a are compared. These two interfaces intensify rapidly at early time and then approach each other while keeping their strength up to a certain distance. At the same time, the mean interior density gradient decreases slightly, as shown in Figure 3-3b. When the two interfaces become close enough, one of them becomes weaker and decays. At this point, the fluid becomes two mixed layers with an interface. The remaining interface also decays and the fluid becomes homogeneous. During this run, the small scale wiggles are also observable. The interfaces are about $5cm$ thick, but the wiggles are about $1.3cm$ thick. The interfaces are thicker than the wiggles so there is no difficulty in telling them apart. Sometimes, the wiggles override the interfaces. This run shows the formation of two coherent interfaces, and an interior layer, characterized by a decrease in density gradient, between the interfaces. The formation of interfaces is not observed during the runs with lower Ri_o such as Run 14. A transition point is expected between the runs with these characteristics and the runs with lower Ri_o.

For a run with even larger Ri_o, interfaces and layers form in the interior as illus-

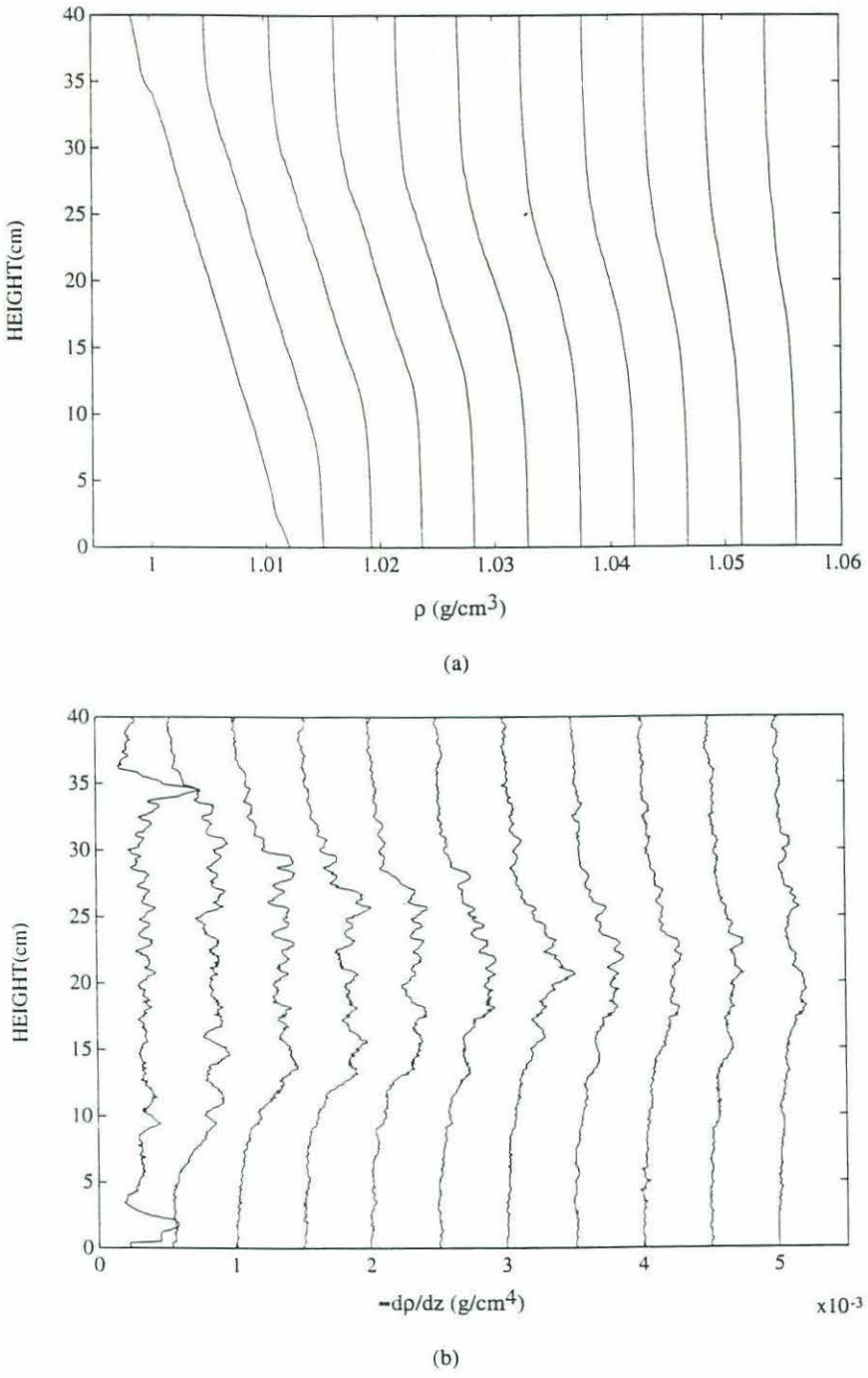

Figure 3-1: The evolution of the density field during Run 14. The values of Re and Ri_o of this run are 547 and 0.31, respectively, and they are below the stability curve in Figure 2-2. (a) The density profile of the initial state and after at every 60 excursions. Each plot is shifted by $0.005 g/cm^3$. (b) The negative of the gradient of the density profiles in (a). Each plot is shifted by $0.0005 g/cm^4$.

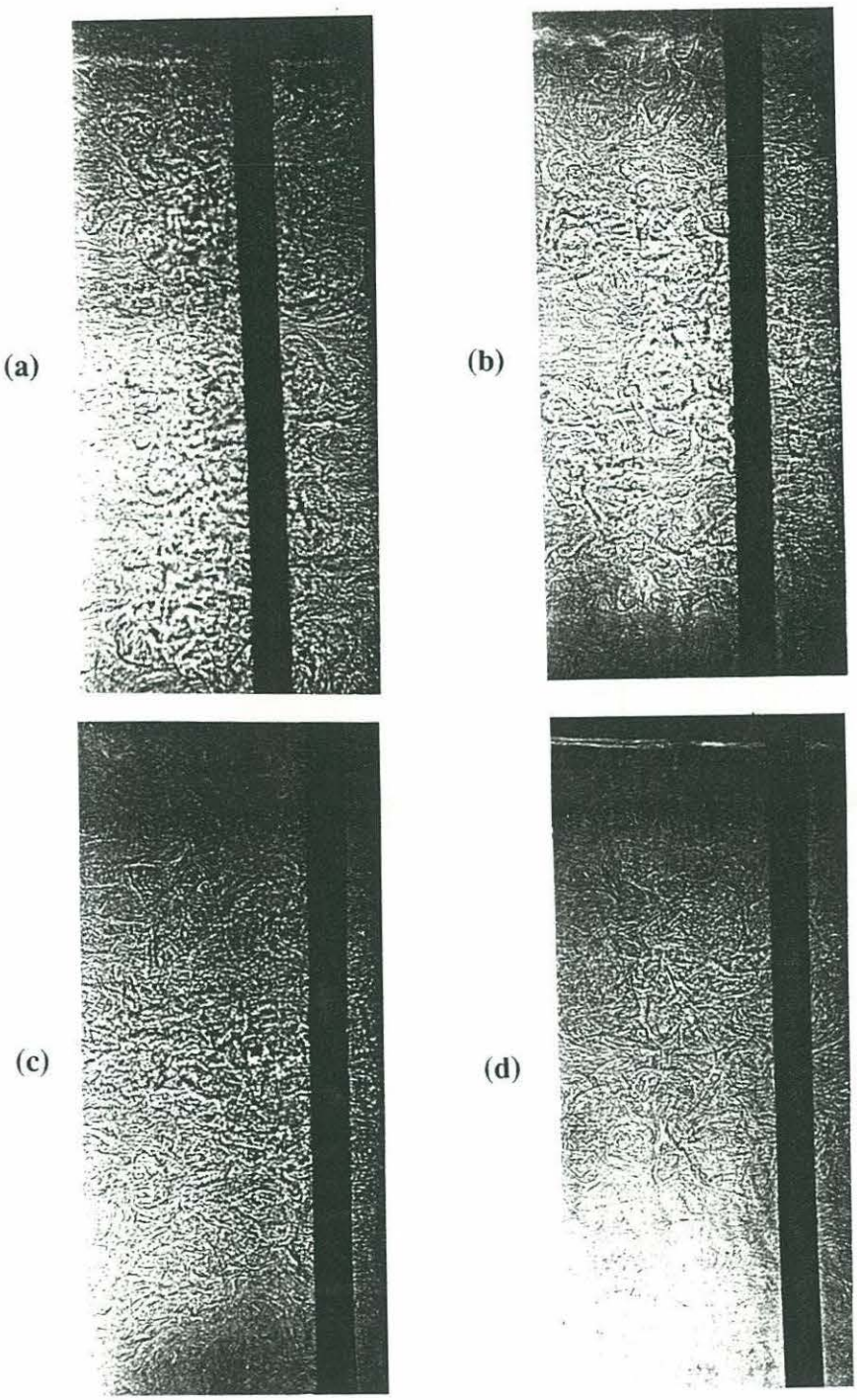

Figure 3-2: A series of shadowgraphs taken during Run 14. The screen was placed about $1m$ in front of the tank. Pictures were taken during (a) $5th$ excursion, (b) $111st$ excursion, (c) $219th$ excursion, and (d) $639th$ excursion. The vertical black strip is the stirring rod with $D = 2.26cm$. The signature of mixing becomes weaker over time. The signature of turbulent mixing is weak near the top and bottom boundaries.

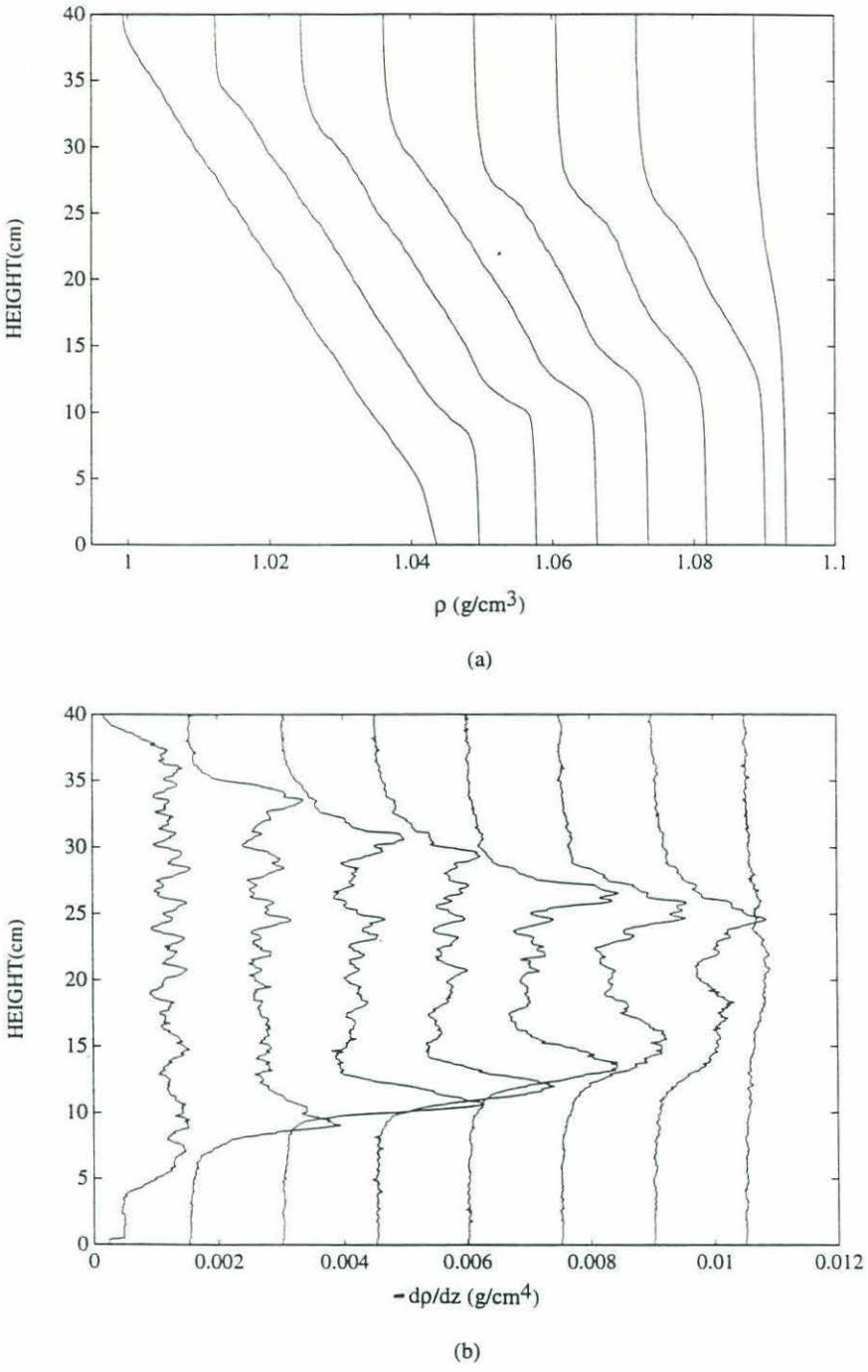

Figure 3-3: The evolution of the density field during Run 13. The values of Re and Ri_o of this run are 547 and 1.04, respectively, and they are slightly above the stability curve in Figure 2-2. (a) The density profile of the initial state and after 150, 300, 450, 750, 950, 1150, and 2250 excursions. Each plot is shifted by $0.01 g/cm^3$. (b) The negative of the gradient of the density profiles in (a). Each plot is shifted by $0.0015 g/cm^4$. The interior mean density gradient slightly decreases over time.

trated in Figure 3-4. In this case (Run 18), Re and Ri_o are 547 and 3.34, respectively. The boundary mixed layers advance rapidly after the beginning of mixing, and then the expansion rate slows down as the interior structure is well established. After this time, the boundary layers do not continue to expand. Instead, the interfaces between the boundary layers and the interior stay at the same position and become weaker while intensifying the adjacent interfaces. The interfaces eventually decay so that the boundary layers show sudden expansion into the interior. The interior density structure changes over time, which is explained in the next section. Figure 3-5 is a series of shadowgraphs taken during Run 17, whose Ri_o of is 2.15 and Re is 547. The interfaces, which are white lines, are maintained under active turbulent mixing. In Figure 8a thin white lines can be seen between the thick white lines. They are the small scale wiggles of about $1.3cm$ thick.

One result of the instability theory of Phillips/Posmentier is the intensification of the interior density gradient if $Ri_o > Ri_c$. If $Ri_o < Ri_c$, turbulence should smooth out perturbations from the mean state so that the formation of a coherent interface or the intensification of density gradient is not possible. Another result of Phillips/Posmentier's theory is a decrease of the density gradient between the interfaces. The evolution of a linear density profile to coherent interfaces while weakening the density gradient between the interfaces, as shown in Figures 3-3b and 3-4c, is defined as a *layering*. The layering is the most clear evidence of the Phillips/Posmentier's instability theory. The stability boundary, which is equivalent to Ri_c, is found by varying Re and Ri_o as shown in Figure 2-2.

In Figure 2-2, the hatched region denotes a marginal region, where a transition from a non-layering to the layering occurs. The layering clearly happens above the marginal region. Below the marginal region the layering is not observed. In the non-layering region, transient interfaces are observed, instead of the coherent interfaces. An example of the transient interface is shown in Figure 3-6 (Run 27). Re and Ri_o are 612 and 0.21, respectively. An interface forms at about $32cm$ after 150 excursions but then decays between 200th and 250th excursion. In the marginal region, the evolution of the density field is not clear. The upper boundary of the marginal region

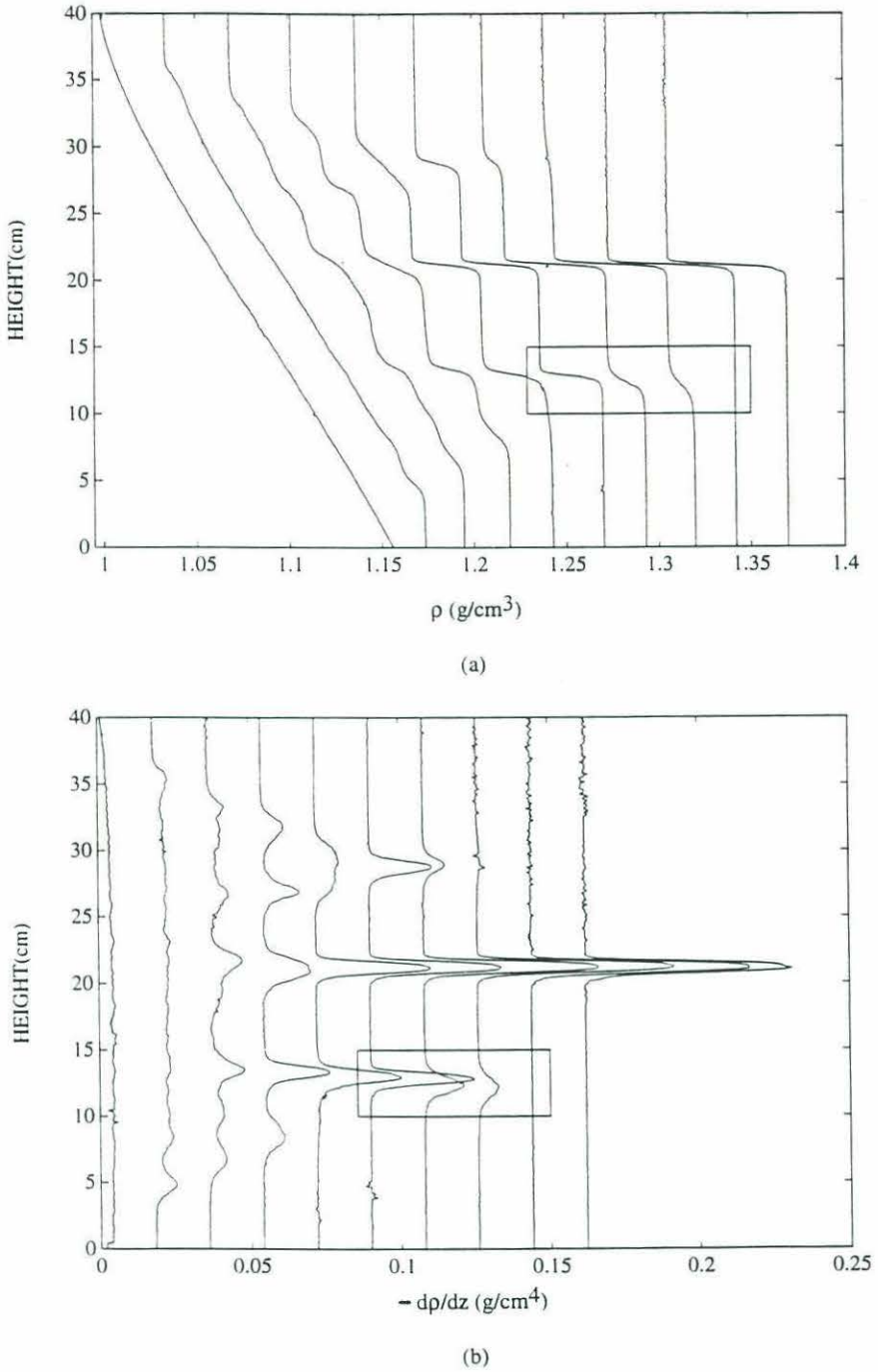

Figure 3-4: The evolution of the density field during Run 18. The values of Re and Ri_o of this run are 547 and 3.34, respectively, and they are far above the stability curve in Figure 2-2. (a) The density profile of the initial state and after 300, 750, 1050, 1500, 1800, 2700, 3000, 3750, and 4500 excursions. Each plot is shifted by $0.01 g/cm^3$. (b) The negative of the gradient of the density profiles in (a). Each plot is shifted by $0.02 g/cm^4$. The boxes in the figures are an example of the decay of an interface. During the decay the interface thickness increases.

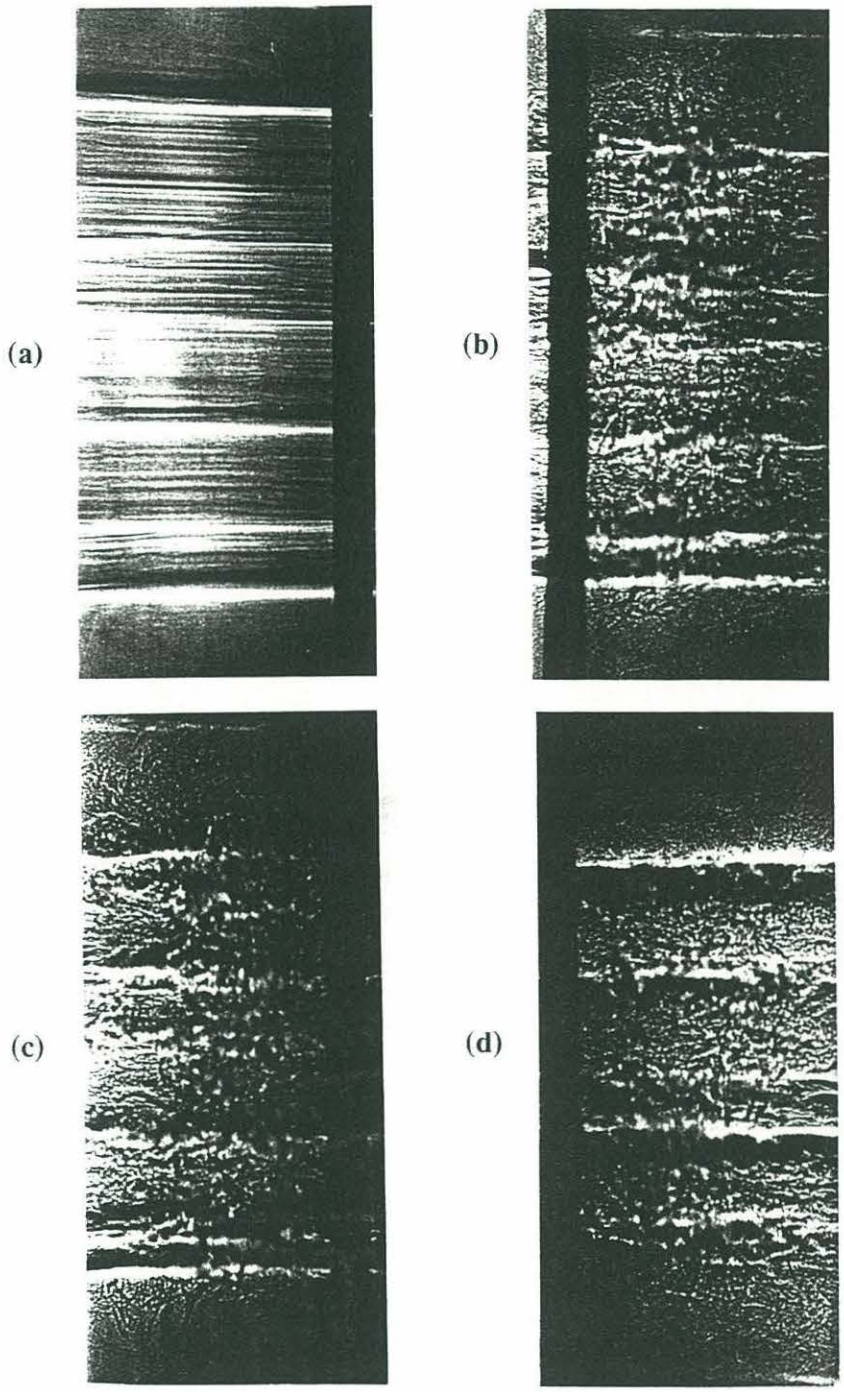

Figure 3-5: A series of shadowgraphs taken during Run 17. The values of Re and Ri_o of this run are 547 and 2.15, respectively, and they are above the stability curve in Figure 2-2. The screen was placed about $1m$ in front of the tank. Pictures were taken during (a) $402nd$ excursion, (b) $582nd$ excursion, (c) $678th$ excursion, and (d) $800th$ excursion. The vertical black strip is the stirring rod with $D = 2.26cm$. The two white strips near the bottom boundary come close over time become one. This is a visual example of the merging of interfaces.

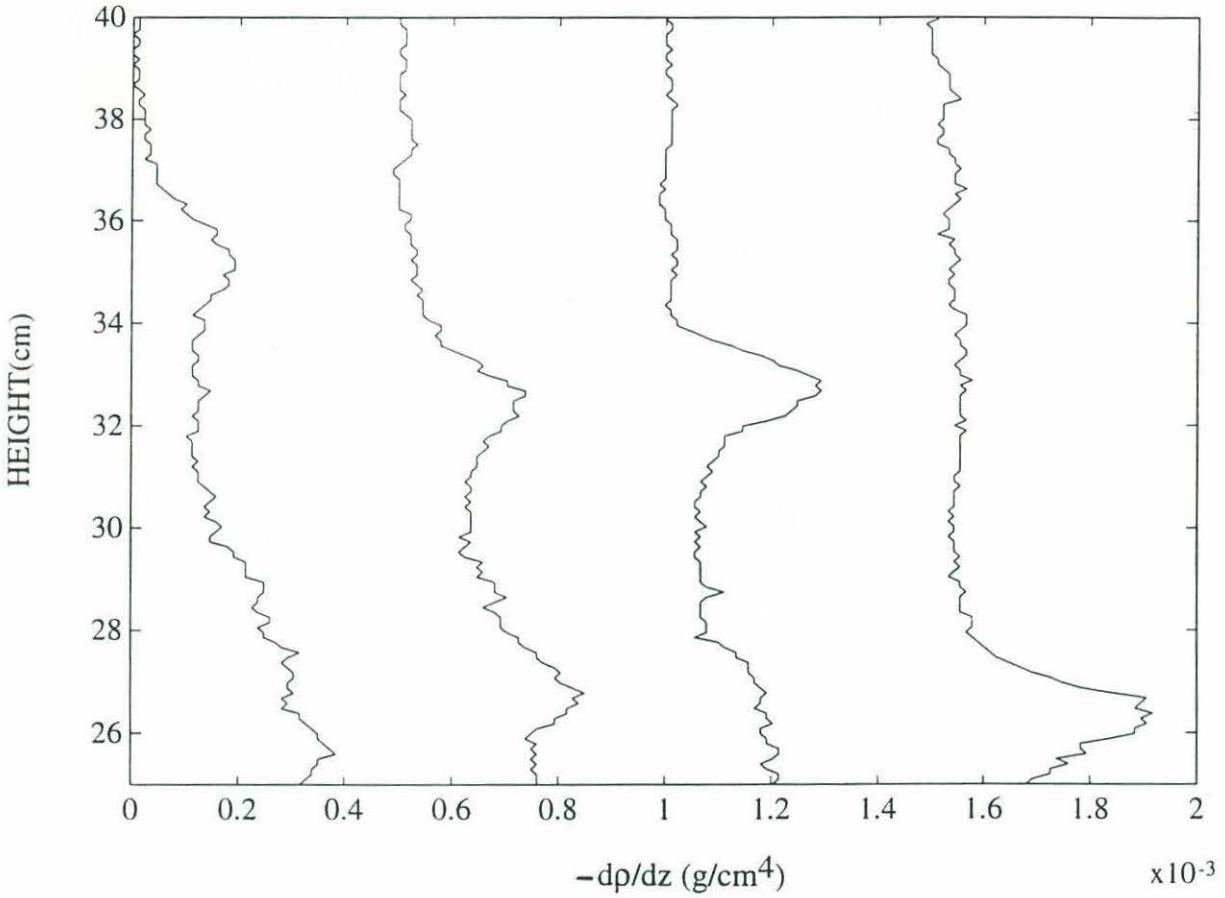

Figure 3-6: The profiles of the negative of the density gradient of Run 27. The values of Re and Ri_o of this run are 612 and 0.21, respectively, and they are below the stability curve in Figure 2-2. The profiles were taken after 100, 150, 200, 250 excursions. Each plot is shifted by $0.0005 g/cm^3$. An interface forms at about $32cm$ but then decays.

is defined as a *stability boundary*, which is Ri_c. The relation between Ri_c and Re is

$$log\, Ri_c \approx \frac{Re}{900},$$

for $400 \lesssim Re \lesssim 1000$.

According to the theory of Posmentier (1977), if Ri_o is slightly larger than Ri_c, the difference between the layer and interfacial density gradients is small. The mixing efficiency, R_f, is high near Ri_c so that the boundary mixed layers might expand rapidly and overtake the interior before interior layering becomes strong enough to be observed. Thus, the present experiments might overestimate the stability boundary.

The overall Richardson number of the stability boundary increases as the Reynolds number increases. For fixed Re, there is a critical Richardson number Ri_c. Thus, in the (Re, Ri_o) parameter space, layering happens when Ri_o increases from zero along constant Re line, and this behavior is consistent with the results. Although, the present experiments cannot find Ri_c precisely, they show the trend clearly. For high Re, due to the rapid advance of boundary mixed layers and high R_f, the marginal region expands as illustrated in Figure 2-2. For high Re, due to the saturation of salt, it was not possible to get $Ri_o > Ri_c$. Thus, increasing Re beyond about 1000 while maintaining the experimental set up is not useful.

3.2 The evolution of the interior layer

For the runs with $Ri_o > Ri_c$, an initially uniform stratification turns into a series of small steps, which become larger and stronger over time. Figures 3-7a and 3-7b, are sequences of the profiles of the density and density gradient taken during Run 4, whose Re and Ri_o are 226 and 2.71, respectively. The steps are in the form of periodic perturbations to the mean density gradient. Naturally, the height of the peaks in density gradient increases by decreasing the density gradient of layers. Figure 3-7 clearly shows the intensification of the interior steps. The sizes of steps increase through a merging or decay of interfaces, which is discussed in the next

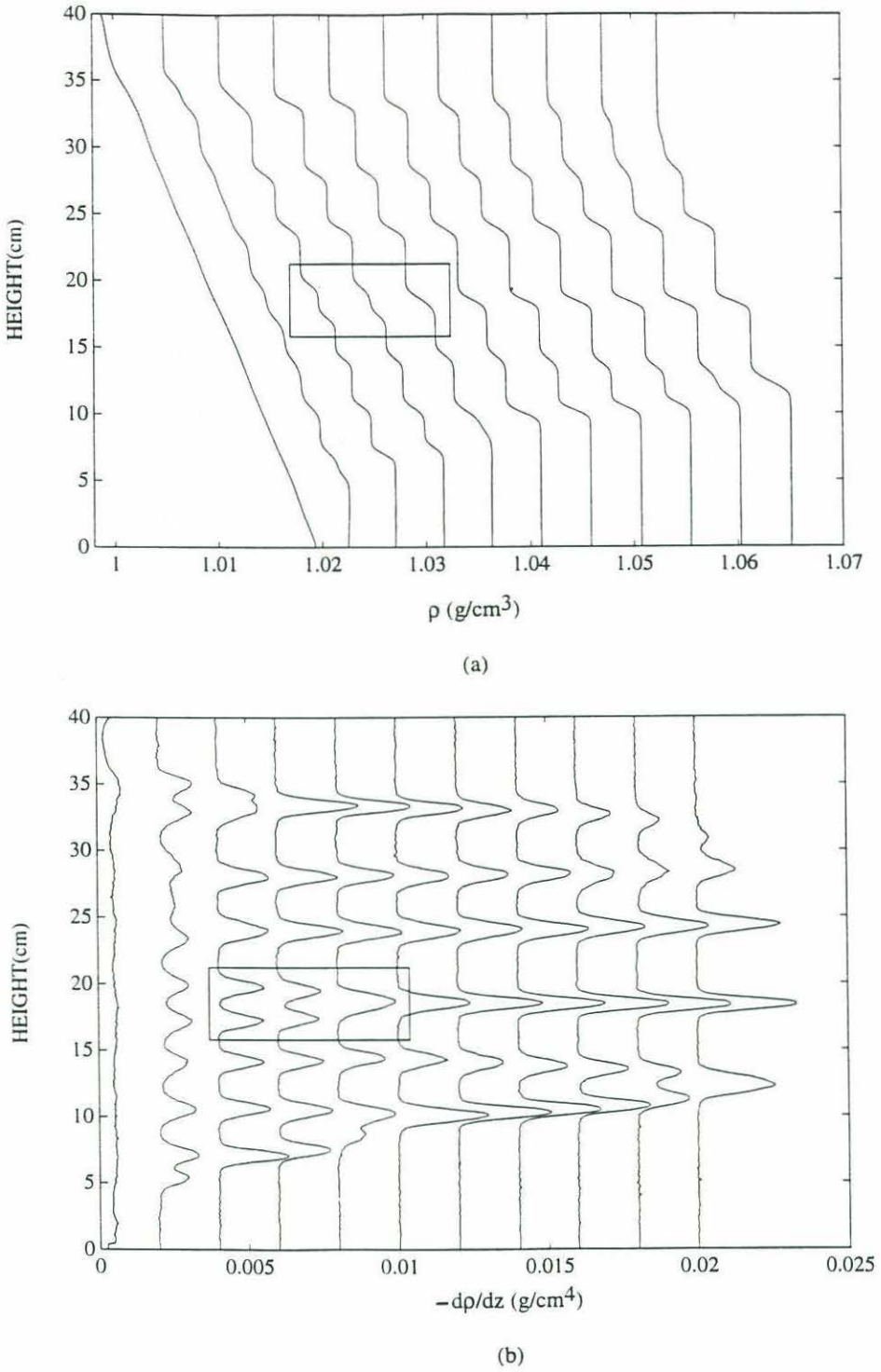

Figure 3-7: The evolution of the density field during Run 4. The values of Re and Ri_o of this run are 226 and 2.71, respectively, and they are above the stability curve in Figure 2-2. (a) The density profile of the initial state and after every 300 excursions. Each plot is shifted by $0.0005 g/cm^3$. (b) The negative of the gradient of the density profiles in (a). Each plot is shifted by $0.002 g/cm^4$. The boxes in the figures are an example of the merging of interfaces.

section, as shown in the figure. Eventually the density profile becomes a series of well-mixed layers with sharp density interfaces. The interior structure seems to reach a *steady state* or an *equilibrium state* after some time. After this time, the merging or decay of interfaces usually happens due to the advance of boundary mixed layers, and the interior almost does not show any evolution. The boundary layers eventually overtake the interior so that the fluid becomes homogeneous.

3.3 The merging and the decay of interfaces

After the initiation of the layering, small layers and interfaces merge and the steps become larger. The *decay* of interfaces was observed and explained by RMT. When the density differences across two adjacent interfaces are different, the density flux across the weak interface is larger according to the theory of Phillips/Posmentier. As a result, divergence occurs at the weak interface, causing eventual decay, while intensifying the adjacent interface. An example of the decay is in Figure 3-8a, which is a sequence of the density gradient profiles of Run 2. The Re and Ri_o of this run are 223 and 0.32, respectively. During the decay both the thickness and positions of the interfaces do not change. The weaker interface just decays. In the interior, the decay is very rare.

The expansion of the boundary layer usually causes the decay of an interface, and the small boxes in the Figures 3-4a and 3-4b are an example. During the decay caused by the expansion of the boundary mixed layers, the interface thickness increases. The decay of interface is also observed at the ends of some runs. For runs with $Ri_o > Ri_c$, the fluid eventually turns into two mixed layers. As time progresses, the density jump across the interface, $\Delta\rho$, decreases slowly while the thickness of the interface remains almost constant as shown in Figure 3-8b, which is a sequence of density profiles taken during Run 18 after the fluid becomes two mixed layers.

The *merging* of interfaces occurs when two interfaces are close, i.e., a layer is thin. The merging happens even when the density differences across two adjacent interfaces are similar so that a divergence of density flux cannot happen. This implies that there

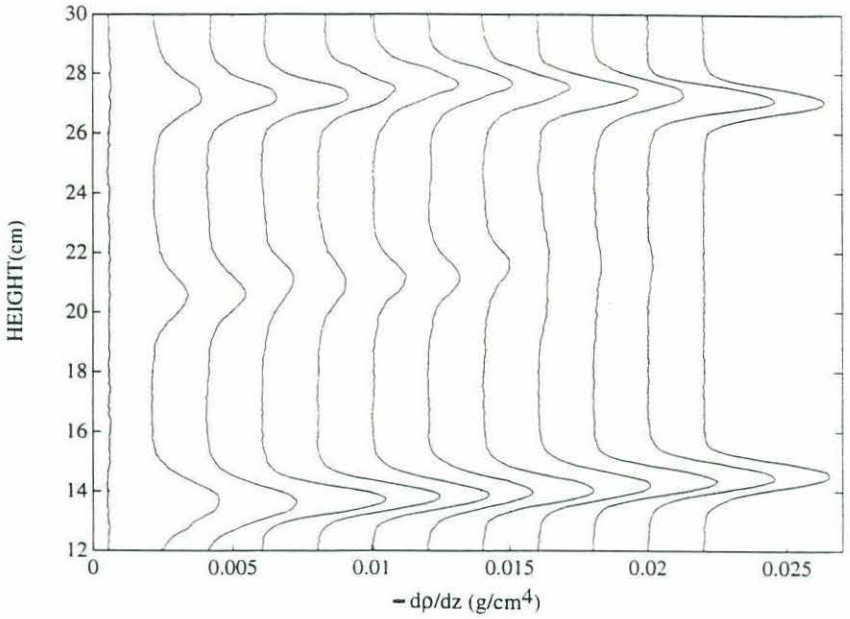

(a)

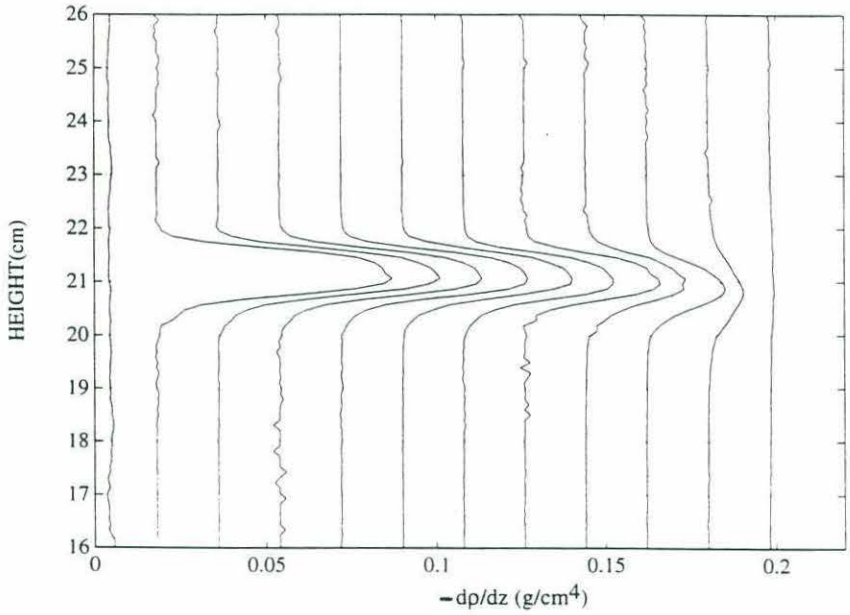

(b)

Figure 3-8: The examples of the decay of interface. (a) The decay of an interior interface during Run 2. The values of Re and Ri_o of this run are 223 and 0.32, respectively, and they are above the stability curve in Figure 3. The negative density gradient profiles of the initial state, after 1000, and then every 200 excursions. Each plot is shifted by $0.002 g/cm^4$. (b) The decay of an interior interface during Run 18. The negative density gradient profiles of the initial state, after 3000, and then every 750 excursions. Each plot is shifted by $0.018 g/cm^4$. The thickness of the interface stays the same until almost the end of the run while the density difference across the interface gradually decreases.

is a minimum length scale of a layer, but the present experiments cannot verify clearly. In the interior, the merging occurs during the early stage of a run. Through merging a new interface forms from the two previous interfaces so the length scale of layer gets larger. The data shows that when the merging occurs, the interface gets thicker and the new interface shows a larger density difference across it. The small boxes in Figures 3-7a and 3-7b are good examples of the merging. The expansion of the boundary mixed layers also cause the merging and Figure 3-5 is a good visual example of the merging. The two white stripes near the bottom of the tank come close and eventually become one.

The merging and decay seem to stop and the interior reaches an equilibrium state. After this state, the decay is usually observed along with the expansion of the boundary layers and the decay of the interior interface is rarely observed. The merging of the interior interfaces is not observed during the equilibrium state.

Chapter 4

Analysis

4.1 The length scale of layers and interfaces

Although the theory of Phillips/Posmentier does not predict any length scale of the steps, the density profiles such as Figure 3-7 shows the existence of one. To find what factors might determine the length scale of steps, the sizes of the steps are compared with the external length scales of the experiments, which are the diameter of the rod, D, and U/N_i. Here, U is the speed of the stirring rod and N_i is the buoyancy frequency of an initial stratification.

Measuring the thicknesses of an interface and an interior mixed layer, separately, is rather ambiguous, since there is no clear border between an interior mixed layer and an interface. But the combined thickness of a layer and an interface can be measured clearly with the plot of vertical density gradient such as Figures 3-3b and 3-4b. The vertical density gradient is a sharp peak at an interface and constant or minimum value in an interior mixed layer. The distance between two adjacent peaks is defined as a *step size*, l_s, when two peaks are of similar sizes. When there are only two interfaces, they approach each other with time due to the expansion of boundary mixed layers. In such cases, the minimum distance that the adjacent peaks achieve before they vanish was considered as a step size as long as the interfaces are the same strength. As explained in section 3.2, the length scale changes with time due to the merging and the advance of the boundary layers. The spacing between the interior

peaks also shows spatial variation. Thus, the minimum distance between two peaks of same strength that do not merge is taken as the step size. In Table 1, the results are listed with the external parameters. The relation between the step size, l_s, and U/N_i is plotted in Figure 4-1.

The size of the step is compared with the external length scales. There are two pairs of runs that have similar parameters except the sizes of rods. One pair is Runs 2 and 5, and the other is Runs 4 and 7. The size of rod, D, is increased 75% and 47%, respectively, but the sizes of step do not change significantly as can be seen in Table 1. As shown in Figure 4-1, the run with $D = 1.29cm$ generate larger step, but the runs with $D = 3.33cm$ generate smaller steps. Runs with $D = 2.26cm$ show large changes in step sizes. It is clear that the sizes of rods do not determine step sizes. On the other hand, l_s and U/N_i show a tendency for a linear relation. The correlation coefficient between l_s and U/N_i is 0.85. In the figure, the solid line is a least square fit to the data. The formula for the line is

$$l_s = 2.6\frac{U}{N_i} + 1.0cm.$$

As Ri_o decreases to the stability boundary by decreasing U/N_i, l_s increases. If the above relation continues to hold down to the stability boundary, l_s becomes comparable to the depth of the tank near the stability boundary. Thus, the depth of the tank becomes a strong obstacle in observing layering. An experiment with a deeper tank is necessary to extend the investigation of the dependence of l_s upon U/N_i down to the stability boundary.

4.2 The spectrum of the density gradient

With the density gradient profile, a spectral analysis was done to see the change of the length scale more clearly. Each profile was divided into 256 subintervals and a Hanning window was applied to each subinterval. Actual calculation was done with Matlab built in function called *spectrum*. Since the data set is finite, the resolution

Run Number	Step Size (cm)	U (cm/sec)	N_i (sec^{-1})	U/N_i (cm)	D (cm)
2	6.6	1.70	0.74	2.29	1.29
4	3.2	1.00	0.73	1.37	2.26
5	6.9	1.70	0.77	2.19	2.26
7	3.2	1.00	0.81	1.23	3.33
9	3.4	1.60	1.68	0.95	3.33
10	3.7	2.77	1.96	1.41	2.26
11	4.0	1.73	2.21	0.78	2.26
15	6.2	2.42	1.30	1.86	2.26
16	7.6	2.42	1.16	2.09	2.26
17	5.5	2.42	1.57	1.54	2.26
18	5.3	2.42	1.96	1.24	2.26
19	4.7	2.02	1.19	1.70	2.26
21	7.1	2.02	0.94	2.14	2.26
22	6.5	2.02	1.06	1.91	2.26
23	6.6	2.02	0.86	2.35	2.26
26	8.8	1.67	0.56	3.00	2.26
28	5.3	1.26	0.54	2.34	2.26
54	5.8	3.24	1.98	1.63	2.26
79	8.7	2.42	1.03	2.34	2.26

Table 4.1: The sizes of steps and the external length scales, D, and U/N_i

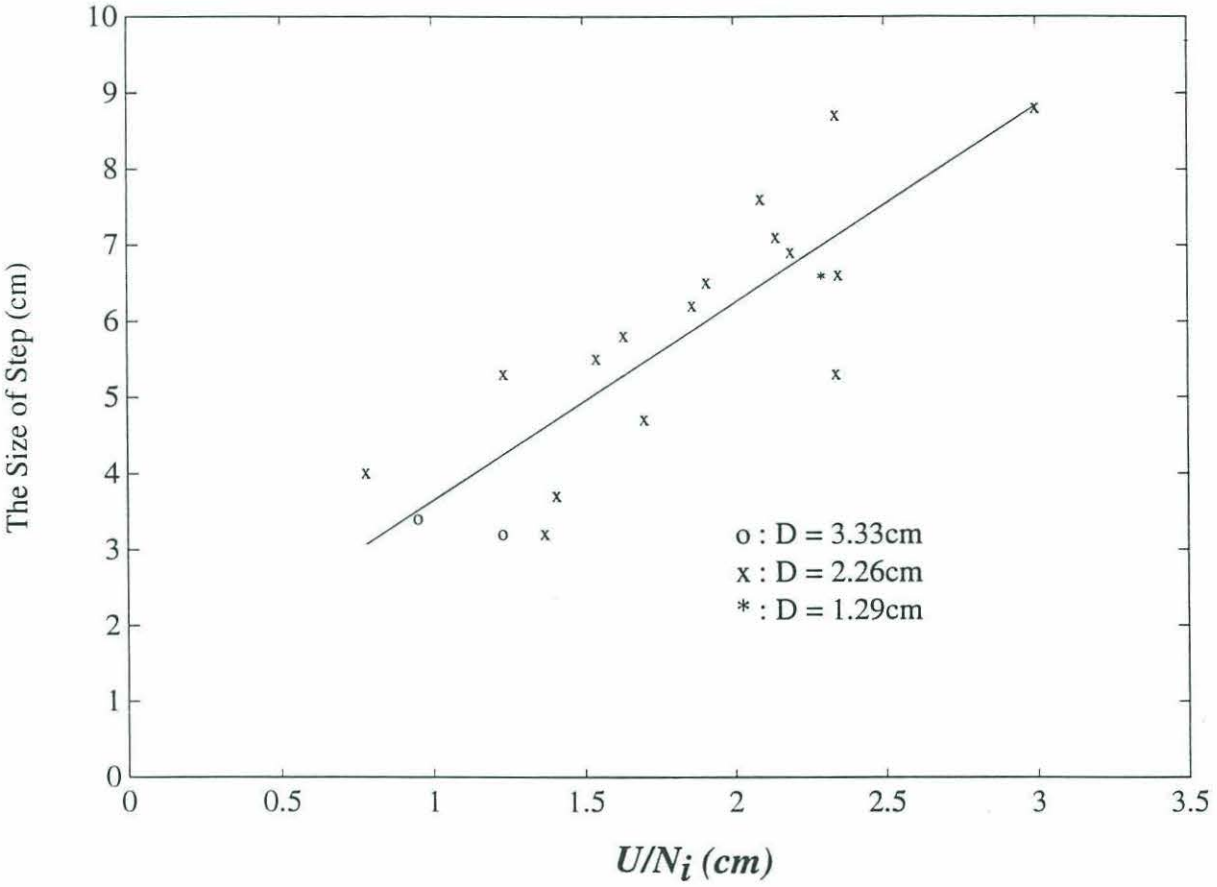

Figure 4-1: The relation between the sizes of the steps and the external parameters, D and U/N_i. The data for this figure is in Table 1. The solid line is the least square fit to the data points. Here, * is for 1.29cm diameter rod, x for 2.26cm rod, and o for 3.33cm rod.

becomes coarse as the length scale increases.

Almost all spectra showed a peak of length scale $1.3cm$ but this does not grow and stays independent of other peaks as shown in Figure 4-2. These small peaks were presumably due to turbulent fluctuations. The presence of these peaks is neglected during the explanation of the spectrum. The spectrum also shows the difference between the layering case and non-layering case. The layering case shows persistent peaks but the non-layering case shows temporally varying peaks as can be seen in Figure 4-2. The initial state is a smooth spectrum in both cases but layering case showed growth of some peaks with time as can be seen in Figure 4-3. The initial peak occurs at relatively short scale and a peak of longer scale occurs later. The short scale peak becomes weaker and eventually the peak of long scale dominates. This state is maintained until the boundary mixed layers overtake the interior. During the second and third cycle of Run 15, spectrum shows a peak at $3.8cm$ as can be seen in Figures 4-3b and 4-3c. During the third cycle, the peak moved to a longer scale, $6.6cm$, as shown in Figure 4-3d. In the figure, the dotted line is the spectrum of sixth cycle. It clearly shows the intensification of the peak at $6.6cm$.

Though the spectrum shows the increase of the step size clearly and consistently with the analysis of Section 4.1, due to the finite size of the data set, this quantification of the length scale is not as useful as the measuring of the spacing between peaks in density gradient, as was done in Section 4.1.

4.3 Energetics

The speed of the stirring rod was known accurately so that the work done to the test fluids was estimated using drag coefficient with the equation

$$\frac{Work\ Done}{one\ Excursion} = \frac{1}{2}\overline{\rho}\, C_d\, U^2 L\, H\, D.$$

Here, H is the depth of the tank, L the length of an excursion, $\overline{\rho}$ the mean density of the fluid, U the speed of the rod, D the diameter of the rod, and C_d drag coefficient. C_d

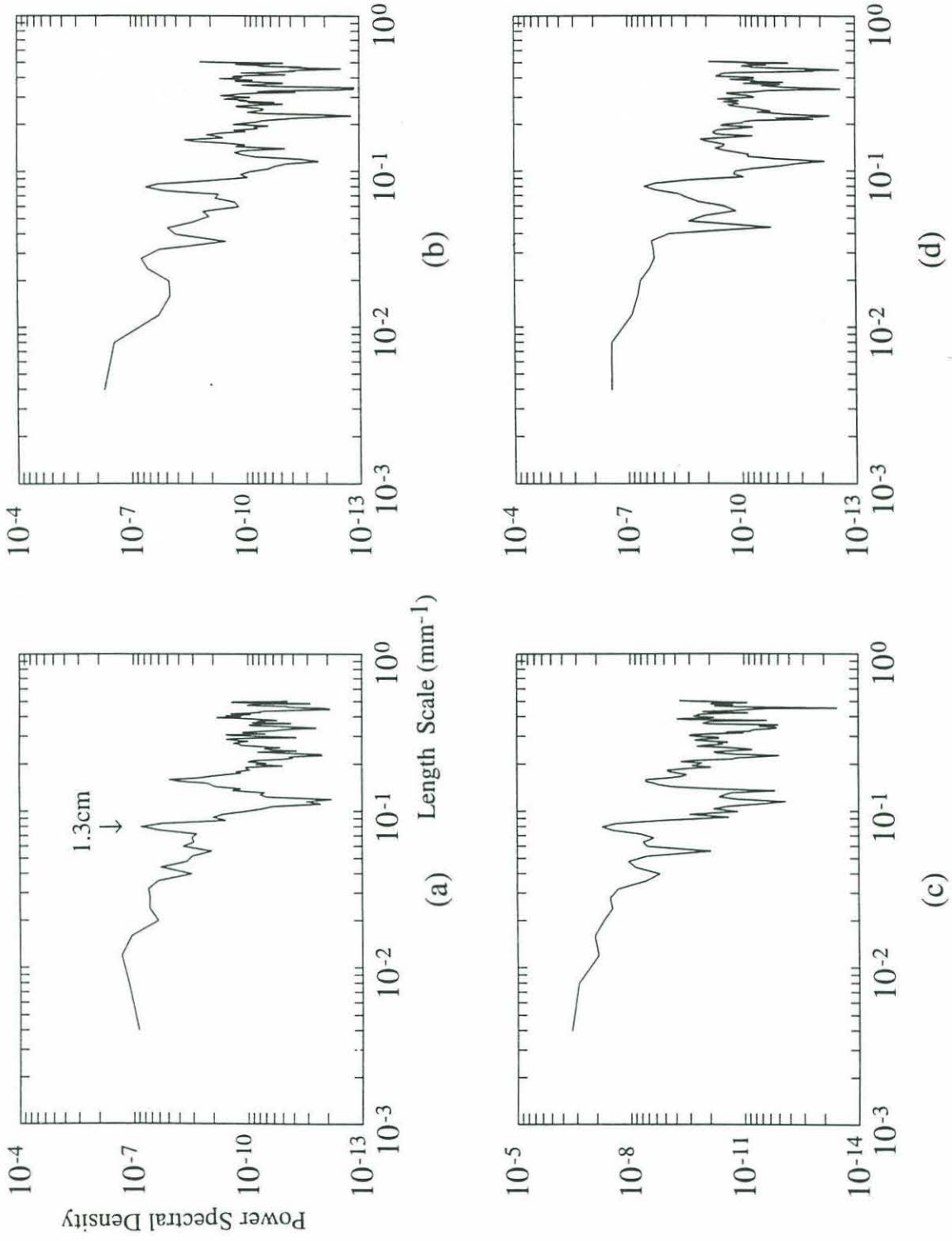

Figure 4-2: The density gradient spectrum of Run 14, one of the non-layering cases. (a) The initial state, after (b) 60, (c) 120, and (d) 180 excursions.

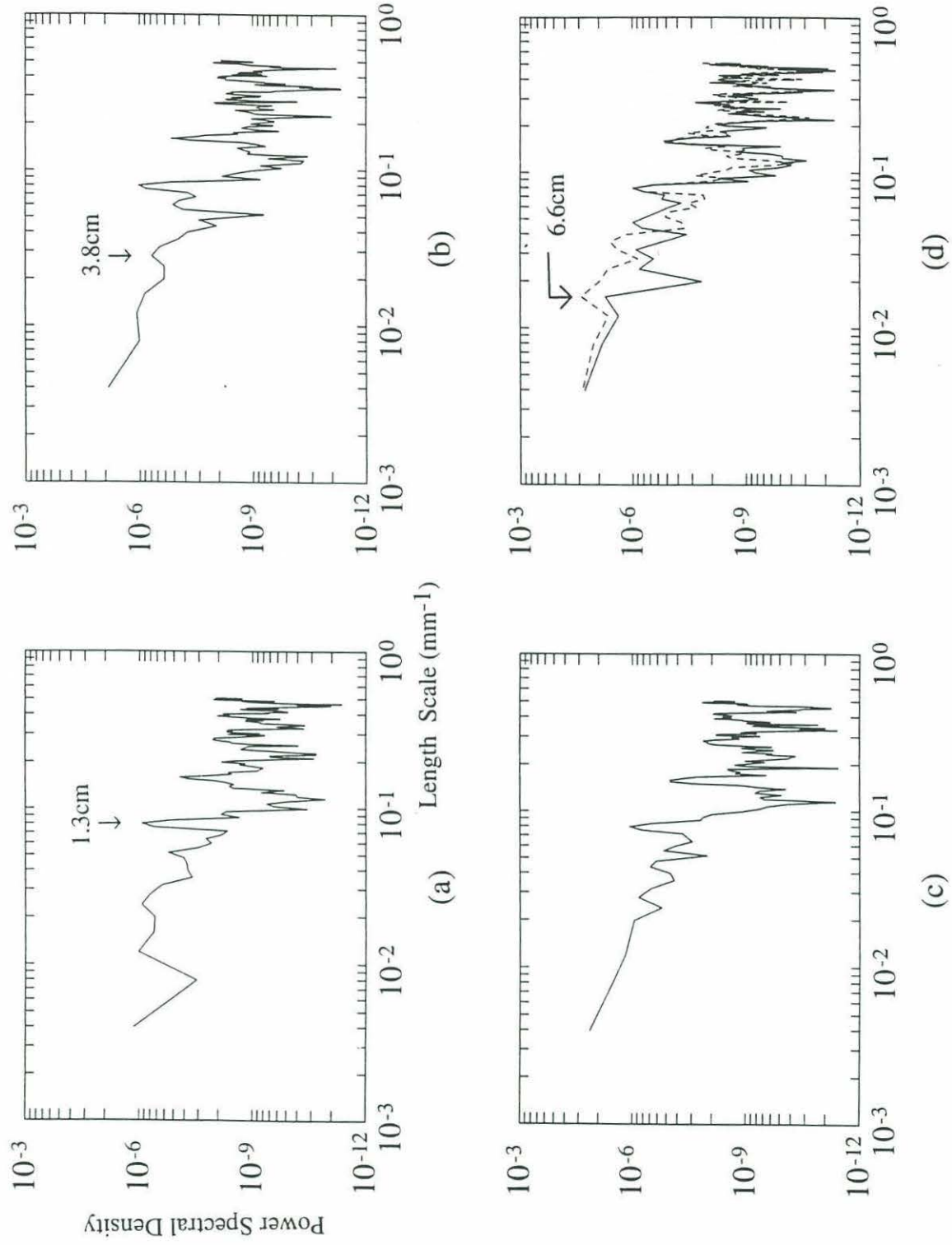

Figure 4-3: The density gradient spectrum of Run 15, one of the layering cases. The values of Re and Ri_o of this run are 547 and 1.47, respectively. (a) The initial state, after (b) 50, (c) 100, and (d) 150 and 300 (the dotted curve) excursions.

was obtained from Figure 5.11.6 in Batchelor (1969). The total work done generated both internal waves of amplitude $1cm$ and turbulence. How much of the work done to the fluid was used to generate the internal waves is not clear. But, a few number of excursions was enough to supply energy for the internal waves. The rod moved perpendicular to the density surfaces and the rod was not a good wave maker. Also, the wave energy cannot radiate out of the tank, so the energy used to generate internal should be far less than that used to make the turbulence.

The total work done must be dissipated in two ways, by friction and by increasing the potential energy of the fluid by mixing the stratification. With the density known at millimeter interval, the change of potential energy of the fluid, $\Delta P.E.$, is calculated using the definition

$$\Delta P.E.(t) = A \int_{bottom}^{top} (\rho_i(z) - \rho(z)) g\, z\, dz.$$

Here, A is the area of the tank, $\rho_i(z)$ the initial density profile, and $\rho(z)$ a density profile measured at later time. The vertical integration was done using the modified Simpson's Rule. The work done and $\Delta P.E.$ are normalized with the difference of potential energy between the initial state and the completely mixed state. The normalization constant of each run is listed in Appendix 2.

With the estimated work done and $\Delta P.E.$ a mixing efficiency, or the flux Richardson number R_f, is defined as

$$R_f = \frac{the\ change\ of\ the\ potential\ energy\ for\ a\ certain\ time\ interval}{work\ done\ to\ the\ fluid\ for\ that\ time\ interval}.$$

As explained before, the work done to the fluid generated some internal waves, which were observed with a shadowgraph, and expected to be dissipated as heat. Because of these internal waves, this definition would underestimate R_f in an oceanic environment.

In the non-layering case, R_f monotonically decreases over time as shown in Fig-

ure 4-4a, which is observed in Run 14. The decrease is probably explained by the expansion of the boundary mixed layers. In these boundary layers, there is little stratification to mix, so the work done to the boundary layers is far more than the potential energy stored in the stratification, and the most of the turbulent kinetic energy is dissipated as heat. As the boundary layers expand an increasing amount of work done on the fluid is dissipated as heat so that R_f decreases along with the expansion of the boundary mixed layers. Figures 3-2b, 3-2c, and 3-2d, which are shadowgraphs taken during Run 14 (a run with $Ri_o < Ri_c$) show the signature of active turbulence mixing in the interior, but the signature of mixing is greatly reduced in boundary mixed layers.

In the layering case, R_f can be divided into three stages of evolution related to the different stages of the density field evolution; 1. the initiation of steps, 2. the equilibrium state, and 3. two layer state. The first stage shows two completely different patterns of R_f evolution. For $Ri_o \gtrsim Ri_c$, there is a decrease of R_f during the first stage as in the non-layering case. But the decrease yields to the second stage, where R_f is rather constant as shown in Figure 4-4b. However, another pattern is seen for $Ri_o \gg Ri_c$, i.e., for Ri_o far away from the stability boundary. In this case R_f sharply increases during the first stage as shown in Figure 4-4c. In Figure 4-5a, for fixed Re, the early changes of R_f are plotted for the different values of Ri_o. As Ri_o increases, the decrease of R_f during the early stage changes to an increase but when the transition occurs is not clear. In Figure 4-5b, the early changes of R_f during the runs with high Ri_o are shown. All of them clearly show the initial increase of R_f.

According to Posmentier (1977), R_f of the equilibrium state should be less than that of the initial state. However, the change of R_f during the development of the steps does not have to be monotonic. Here, it is not clear whether the decrease verifies the prediction of the theory, or the decrease is due to the expansion of the boundary mixed layers. The initial increase seems to contradict Posmentier's theory. Turner (1973) discussed the energetics of layering in the presence of turbulence. Initially, stratification is so large that turbulence cannot mix the stratification effectively. By developing a step-like density structure, the local gradient Richardson

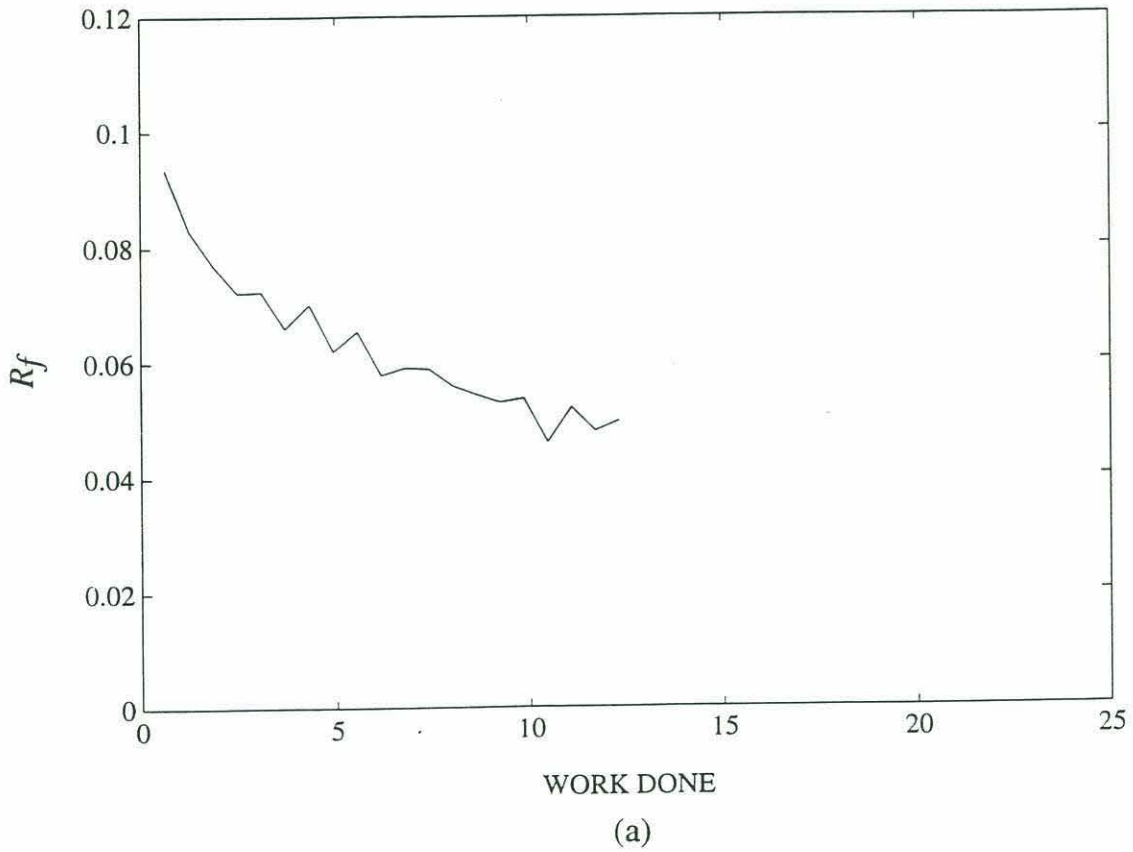

Figure 4-4: The mixing efficiency, R_f, versus work done. (a) Run 14. Here, $Ri_o < Ri_c$. R_f decreases monotonically to the end of the run. (b) Run 5. Here, $Ri_o > Ri_c$. (c) Run 18. Here, $Ri_o \gg Ri_c$. In (b) and (c), R_f shows three different stages of evolution. In (b) R_f decreases initially, but in (c) R_f increases initially. In (b) the second stage is clear, but in (c) the second stage is contaminated by the merging and decay of interfaces due to the advance of the boundary mixed layers.

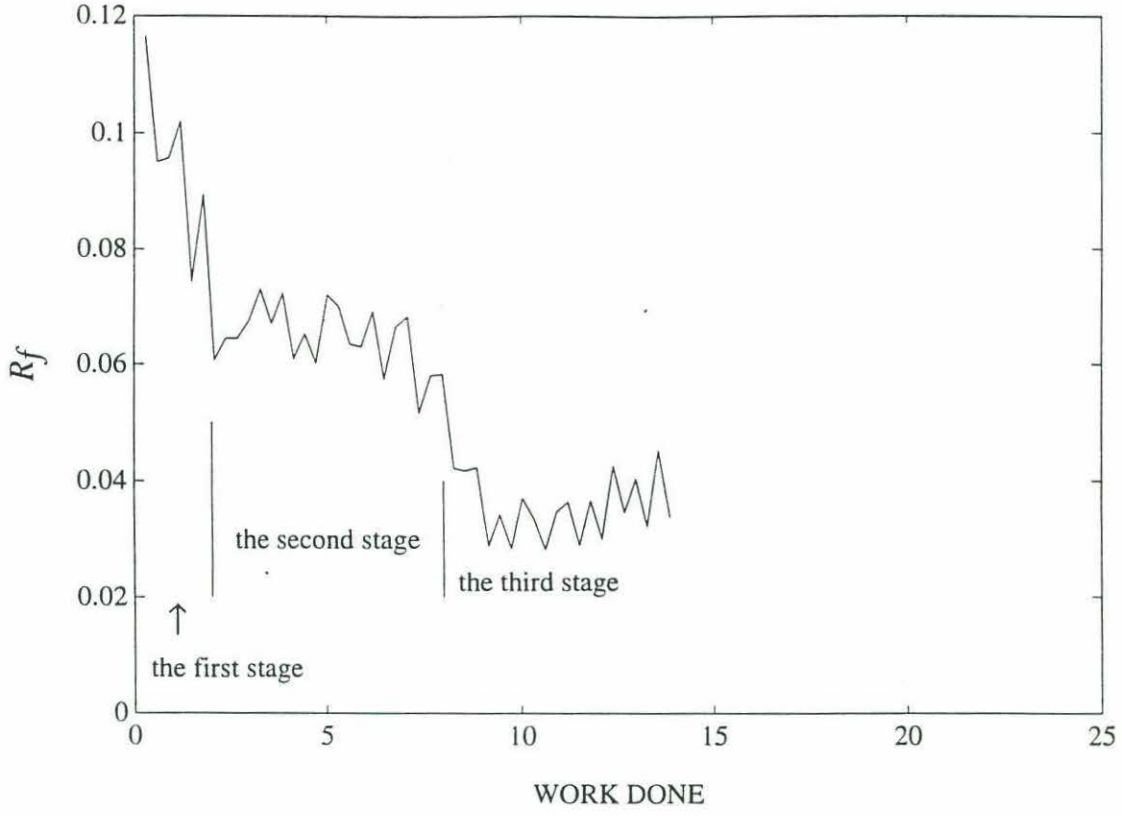
0.12
0.1
0.08
0.06
0.04
0.02
0
Rf
the second stage
the third stage
the first stage
0
5
10
15
20
25
WORK DONE

(b)

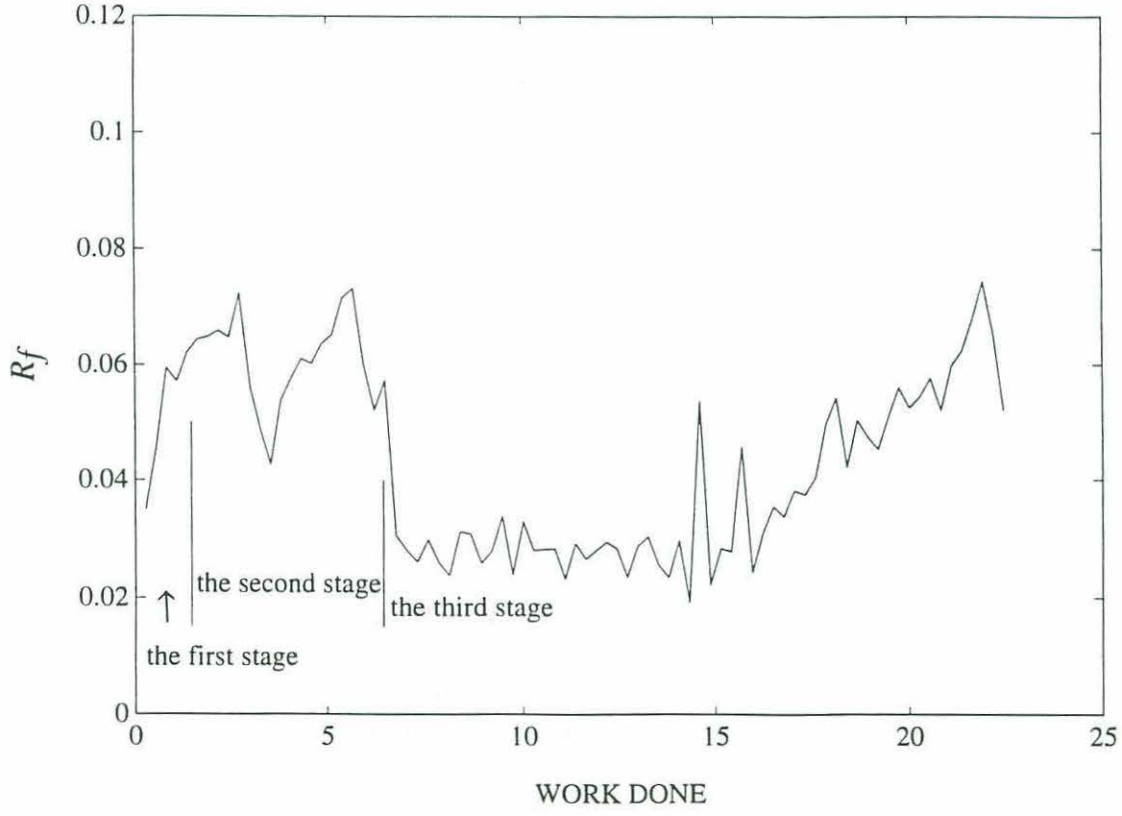
0.12
0.1
0.08
0.06
0.04
0.02
0
Rf
the second stage
the third stage
the first stage
0
5
10
15
20
25
WORK DONE

(c)

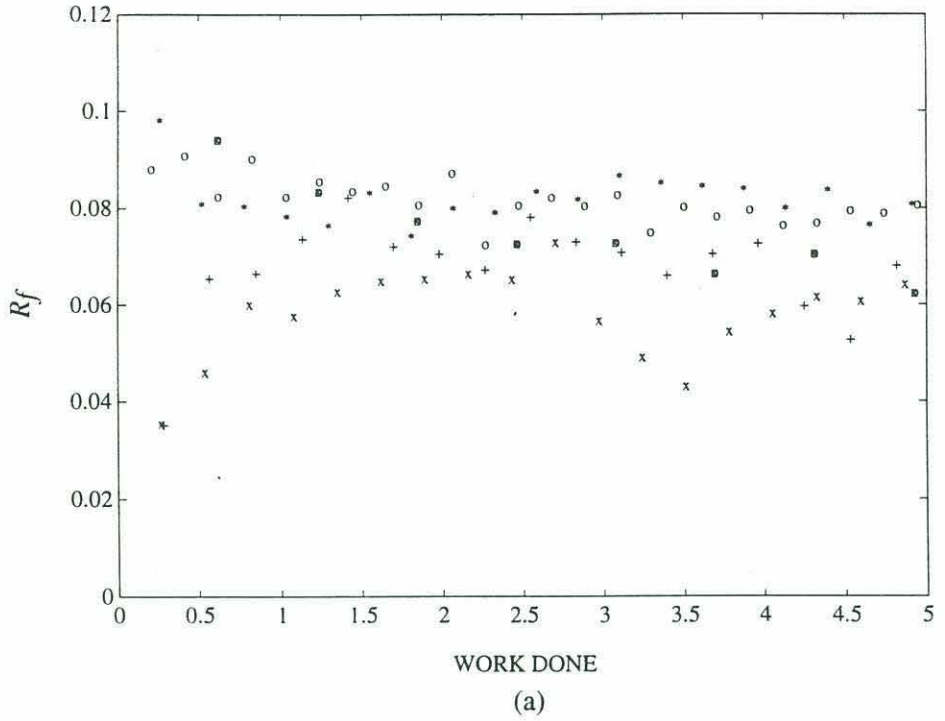

(a)

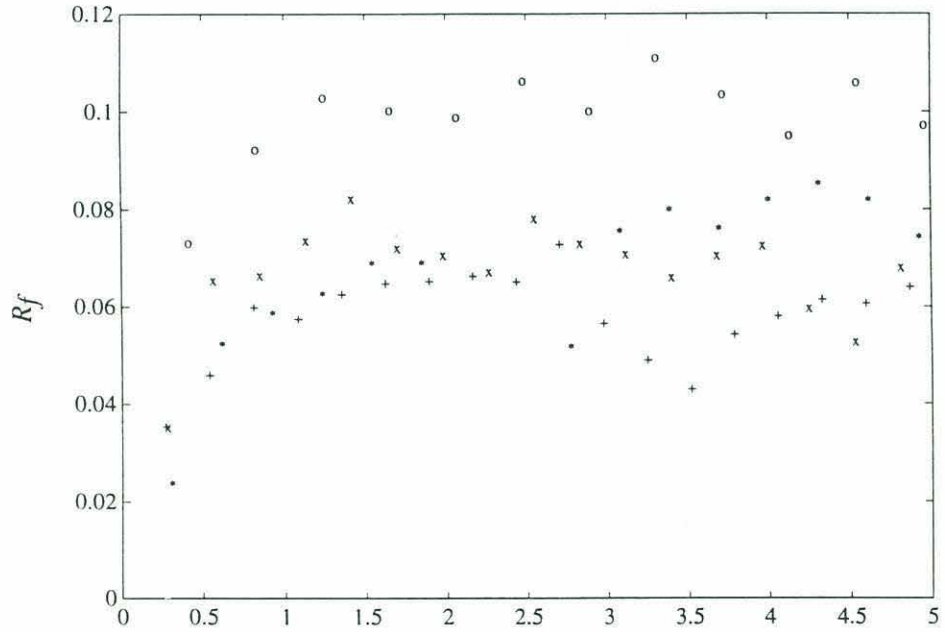

(b)

Figure 4-5: Examples of the initial change of R_f. (a) Re is fixed at 547. Ri_o is x:3.3 (Run 18), +:2.2 (Run 17), o:1.5 (Run 15), *:1.2 (Run 16), and ◙:0.3 (Run 14). For $Ri_o > Ri_c$, R_f shows a decrease. However, for $Ri_o \gg Ri_c$, R_f shows a sharp initial increase. (b) For $Ri_o \gg Ri_c$. All of them show the initial increase. The values of Re and Ri_o of each case are +:547, 3.3 (Run 18), x:547, 2.2 (Run 17), *:730, 1.9 (Run 54), and o:860, 1.4 (Run 58), respectively.

number is reduced locally to a value at which turbulent mixing can be maintained. One consequence of this discussion is that during the formation of steps more mixing is allowed in the layers so that the mixing efficiency increases, which is observed with the runs of $Ri_o \gg Ri_c$.

A characteristic of the second stage is a nearly constant R_f. In Figure 4-4b, the second stage is clear but some runs do not have a long enough time for this stage to be evident. Also the expansion of the boundary mixed layers cause a merging or decay of interfaces, and contaminates the characteristics as shown in Figure 4-4c. During this stage, the interior density structure is nearly unchanged.

The border between the second and third stages is clear. R_f sharply decreases. The advance of the boundary mixed layers result in two mixed layers with a strong interface between them. A sharp decrease of R_f is observed between the border of the second and third stages. This phenomenon indirectly supports the relation that R_f decreases as Ri_o increases beyond Ri_c. During the third stage R_f is nearly constant as shown in Figure 4-3c, and the experiments become equivalent to the turbulent entrainment experiments such as Turner (1968) and Linden (1980). Eventually, the remaining interface also decays, resulting in an increase of R_f, which is discussed in the next section, as shown in Figure 4-4c.

As explained before, the relation between R_f and Ri is the most important assumption of the stability theory. With the third stage of Runs 17 and 18, i.e., after the fluid became two well-mixed layers, the relation between R_f and the local Richardson number Ri_l is found. The definition of Ri_l is

$$Ri_l = \frac{g\Delta\rho l}{\overline{\rho}U^2},$$

where, l is the length scale of turbulence, and $\Delta\rho$ the density difference across the interface. The length scale of turbulence was not measured so that the determination of l as defined above is not possible. Instead the thickness of the interface is used for l. The results are shown in Figure 4-5. R_f decreases clearly as Ri_l increases, and R_f becomes nearly constant for $Ri_l \gtrsim 10$. The present experiment was not designed

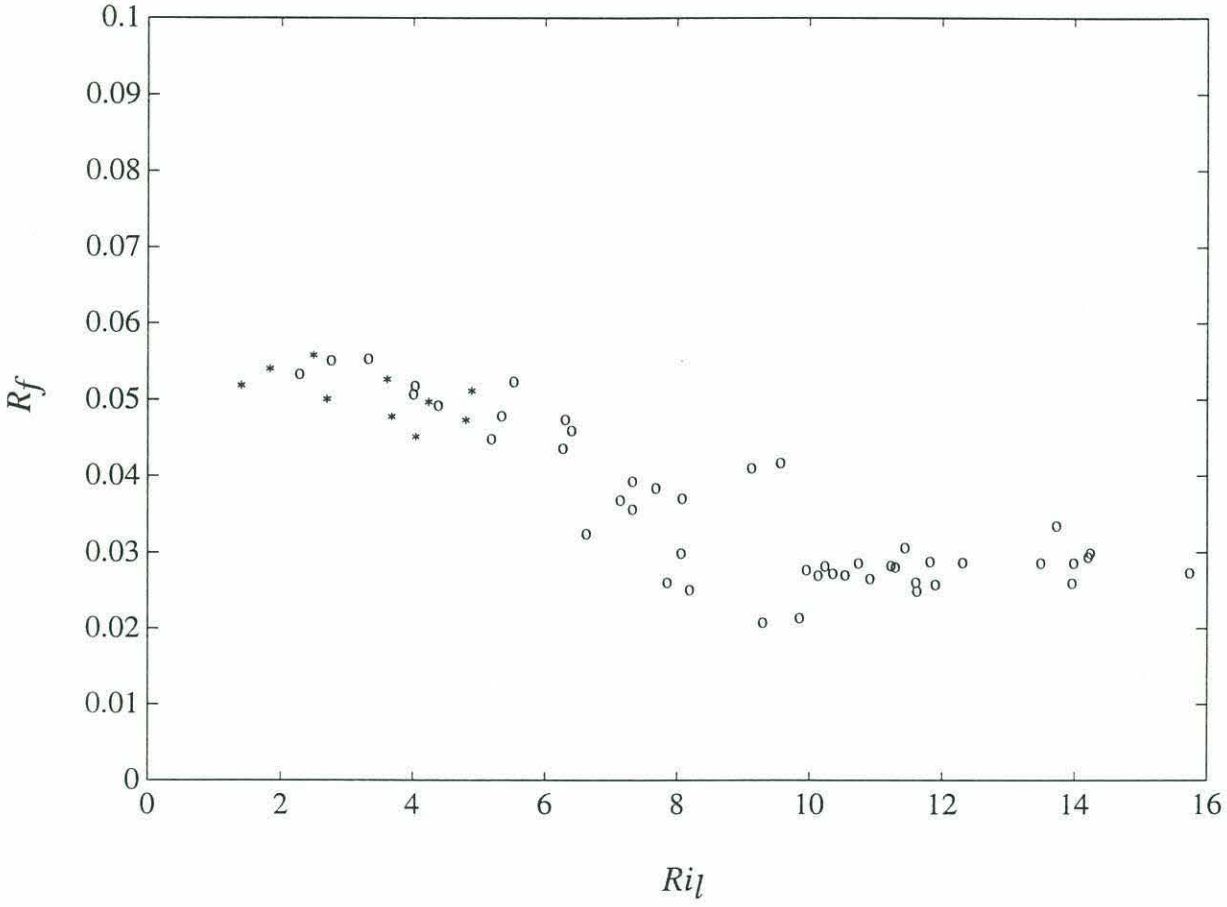

Figure 4-6: Ri_l versus R_f. The data during the third stage of Runs 17 and 18 are used. R_f decreases as Ri_l increases and becomes nearly constant for $Ri_l > 10$. Here, * denotes Run 17, and o Run 18.

to find the relation between R_f and Ri_l so that the increase of R_f from zero as Ri_l increases from zero cannot be found. As Ri_l approaches to zero by decreasing $\Delta\rho$, R_f should become zero and the increase of R_f as Ri_l increases from zero can be inferred. Some runs show a decrease of R_f during the decay of the final interface and this implies the decrease of R_f as Ri_l approaches to zero.

Both the non-layering cases and layering cases near the stability boundary show a rapid decrease of mixing efficiency during the early stage of the runs. The decrease is presumably due to the expansion of the boundary mixed layers, in part. Unfortunately, the density profile was not measured often enough to show the very early change of R_f.

4.4 Density flux

Vertical density flux was calculated using mass conservation. The horizontal average of the mass conservation equation is

$$\frac{\partial}{\partial t}\overline{\rho}(z,t) = -\frac{\partial}{\partial z}F(z,t).$$

Here, the overbar denotes horizontal averaging, and $F(z,t)$ is the vertical density flux. Since the density flux is zero at the horizontal boundaries, vertical integration of the above equation gives

$$F(z,t) = \int_z^{top} \frac{\partial\overline{\rho}(z',t)}{\partial t}\, dz'.$$

Since the density profile was measured after active turbulence decayed, the measured density profile was a horizontal average. Integration was done from the top of the tank. The difference between the two density profiles of before and after a certain cycle was used for the time differentiation. The calculation satisfies the no flux condition at the other boundary within a very small error. This shows that both the calculation and

probe drift correction were very accurate. In addition, the density flux calculation does not contain any ambiguous estimation such as the work done estimation.

The vertical integral of the density flux times g, the gravitational acceleration, gives the time differentiation of potential energy change. The density flux calculated in this way has been found to be consistent with the mixing efficiency analysis in section 4.3. In non-layering case, the interior density structure changes very slowly as explained in section 3.1 so that a uniform density flux is expected in the interior. The density flux contours of a non-layering case are shown in Figure 4-7. The figure does show a region, which shrinks over time, of nearly uniform density flux. At the horizontal boundaries, the density flux should become zero, and in the boundary mixed layers the density gradient is almost zero. Thus the profile of the density flux shows a shape of a plateau. As the boundary mixed layers expand, the width of plateau decreases while its height stays nearly the same. This causes the monotonic decrease of R_f as shown in Figure 4-4a.

The most prominent feature of the layering case is that the density flux is uniform in the layered interior as shown in Figure 4-8a, though the density gradient varies greatly in the interior as shown in Figure 4-8b. This supports the theory of Posmentier(1977) most clearly, since the density flux should be constant regardless of the density gradient. The divergence of the density flux is quite small as long as the interior structure stays the same. At the bottom boundary mixed layer a density flux is generated, and the flux goes through the interior all the way from the bottom to the top without changing the interior density structure. It shows that turbulence can transport scalar properties such as heat, salt, or density further than the length scale of turbulent eddies without changing the structure of the stratification.

The merging of interfaces results in a local maximum of density flux in time and space. The small boxes in Figures 4-8a and 4-8b are an example. When the merging happens the thickness of the interfaces increases as explained in section 3.3. Linden(1979) showed that an increase of an interface thickness causes a local increase of a density flux. As an interface becomes thicker, the density gradient of the interface decreases so that turbulent mixing becomes more effective if the Ri_l of the interface

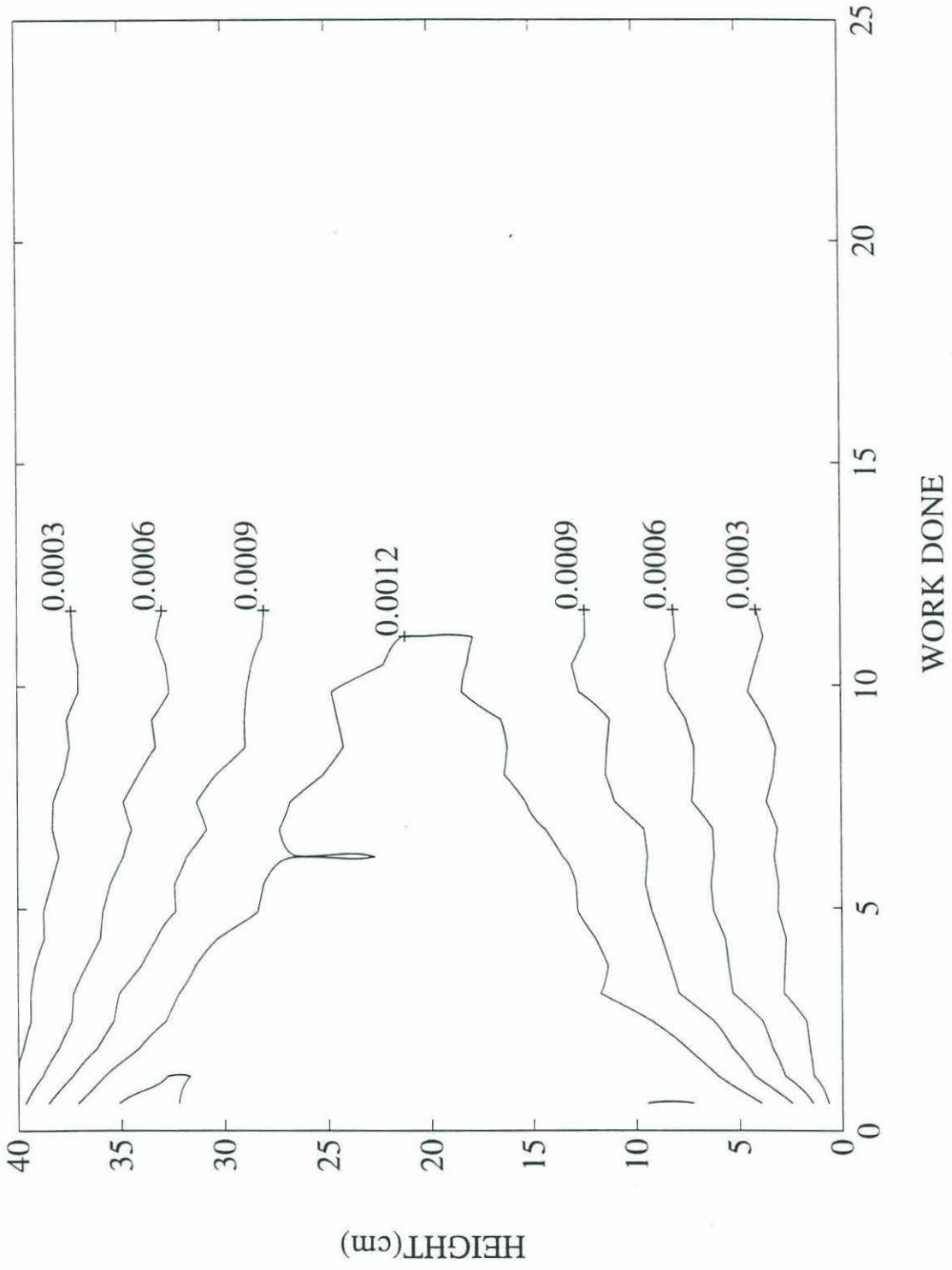

Figure 4-7: The density flux contours of Run 14. The unit of the contours is in g/sec. In the interior the density flux is approximately uniform. The interior density gradient is also uniform as shown in Figure 3-1b.

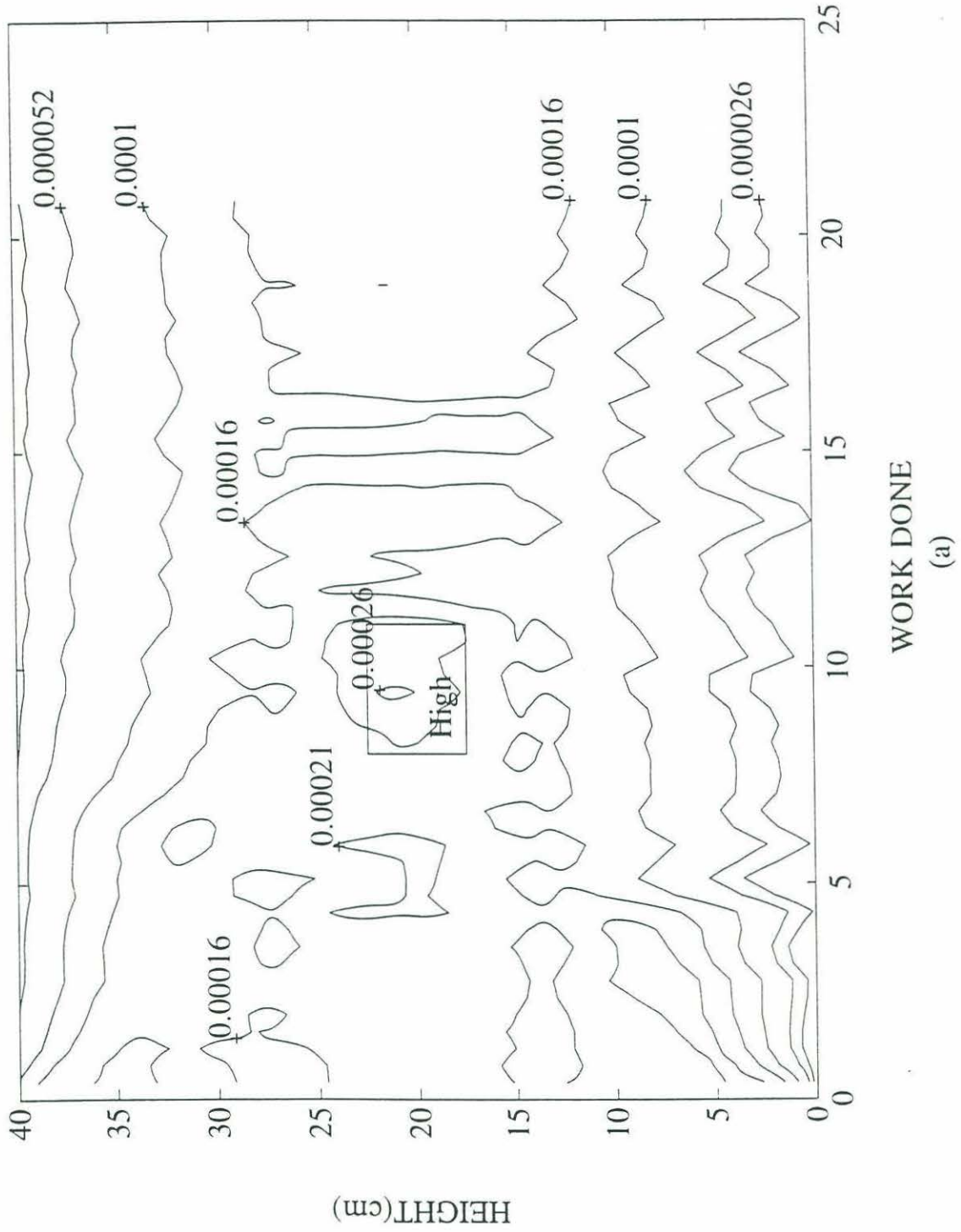

Figure 4-8: (a) The density flux contours of Run 2. The unit of the contours is in $g/sec.$ (b) The density gradient contours of the run. The unit of the contours is in g/cm^4. The small boxes in the figures are an example of the local maximum of the density flux during the decay of an interface. The density flux shows a local maximum when work done is about 10 and the height is about $20cm$, at which the decay of an interface occurs. The density flux is uniform in the layered interior, regardless of the density gradient.

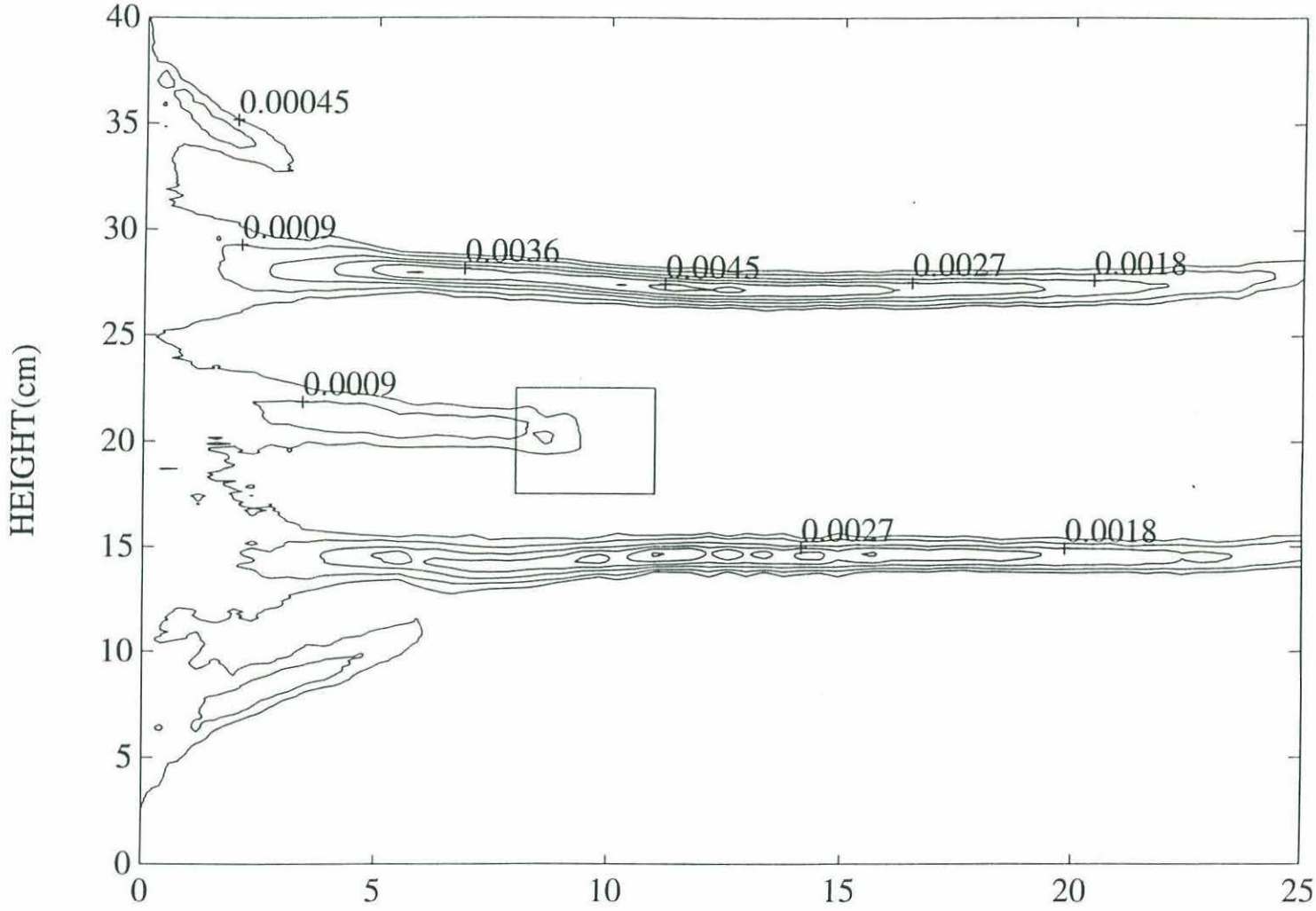
40
35
30
25
20
15
10
5
0
0
5
10
15
20
25
HEIGHT(cm)
WORK DONE
0.00045
0.0009
0.0036
0.0045
0.0027
0.0018
0.0009
0.0027
0.0018

(b)

is larger than Ri_c. Secondly, the density difference across the interface disperses vertically so that more of the turbulent kinetic energy is used to mix the density difference. Thus, the mixing efficiency increases. The increase of the density flux, F, also can be explained using the relation between R_f and Ri. During the merging, Ri of interfaces decreases so that R_f increases. At the layer between the interfaces Ri locally increase, which causes a local increase of R_f. After the merging a stronger interface is formed as explained in section 3.3, and Ri of the new interface increases beyond those of interfaces before the merging and R_f decreases locally. Thus the merging shows a local maximum in the density flux.

The decay of an interface also shows a local maximum. The density gradient of an interface decreases during the decay and Ri, too. Turbulence can mix the density field more efficiently since Ri of the interface is larger than Ri_c, and the density flux increases locally. During the decay of an interface, somewhere within the interface there should be a point where $\partial\rho/\partial t = -\partial F(z,t)/\partial z = 0$. This means a spatial extremum of F. Since the magnitude of the gradient decreases

$$\frac{\partial}{\partial t}\frac{\partial \rho}{\partial z} = -\frac{\partial^2 F}{\partial z^2} > 0,$$

so the extremum is a maximum.

With the strongest interface formed during the present experiments, the molecular diffusive flux and the turbulent flux are compared. The molecular diffusive flux $F_d = \kappa_s \Delta\rho/d$. Here κ_s is the molecular diffusivity of a salt, $\Delta\rho$ is the density difference across the interface, and d is the thickness of the interface. In the present experiments the maximum value of $\Delta\rho$ is $0.066\, g/cm^3$, D is $2\, cm$, and κ_s is $1.5 \times 10^{-5} cm^2/sec$. So, F_d is about $1 \times 10^{-4}\, g/sec$. The turbulent density flux is more than $1 \times 10^{-3}\, g/sec$, which is 10 times larger than the molecular diffusive flux. Even at the strongest interface the turbulent flux dominates.

Chapter 5

Conclusions

A linearly stratified fluid was mixed with a rod moving horizontally at a constant speed. The initially uniform density profile evolves into steps when the overall Richardson number, Ri_o, is large and the Reynolds number of the rod, Re, is small. By changing Re and Ri_o the stability boundary of layer formation was found. The stability boundary is consistent with the relation between the mixing efficiency, R_f, and Ri_o. The higher Re is, the higher Ri_o is required to see the layering. The relation between the stability boundary, Ri_c, and Re is

$$log\, Ri_c \approx \frac{Re}{900},$$

for $400 \lesssim Re \lesssim 1000$.

The steps evolve over time. Small steps form first, and they become larger through the merging and decay of interfaces. The merging occurs between two closely spaced interfaces. This implies that there might be a minimum step size but the present experiments cannot verify the idea. The interior seems to reach an equilibrium state. The merging or decay of interfaces usually occurs due to the advance of boundary mixed layers after the interior reaches the equilibrium state. Thus, the interior structure seems to be unchanged after some time, if there is no expansion of the boundary mixed layers. The size of the equilibrium steps, l_s, is a linear function of the external

length scale U/N_i, and the relation is

$$l_s = 2.6\frac{U}{N_i} + 1.0\,cm.$$

The analysis of the energetics shows that for $Ri_o > Ri_c$, the change of R_f is closely related to the formation and decay of steps. While the non-layering case shows a monotonic decrease of R_f throughout a run, the layering case shows three different stages. During the initiation of steps, depending on Ri_o, R_f shows two completely different patterns of time change. For $Ri_o \gtrsim Ri_c$, R_f decreases initially. Posmentier (1977) shows that R_f of fully developed steps is smaller than that of the initial state. The expansion of the boundary mixed layers always decreases R_f and the present experiments cannot verify the decrease of R_f, which Posmentier predicted, after layer formation. An experiment with a constant boundary flux is necessary to verify the decrease.

For $Ri_o \gg Ri_c$, R_f sharply increases initially, however. The increase is contradictory to the theory of Phillips/Posmentier. Turner (1973) argues that if stratification is too strong to maintain turbulence, then by developing a step-like density structure the local gradient Richardson number is reduced locally to a value at which turbulent mixing can be maintained. Thus, R_f increases as the steps develop. The observed increase of R_f seems to support this argument.

When the steps reach an equilibrium state, R_f becomes uniform regardless of the initial behavior as long as the interior steps are maintained. R_f goes through a sharp decrease as the fluid becomes two mixed layers, then becomes uniform.

The relation between R_f and Ri_l, the local Richardson number based on the thickness of an interface, is found with the density profiles after the fluid becomes two mixed layers. R_f decreases uniformly as Ri_l increases for $Ri_l \gtrsim 1$. For $Ri_l \gtrsim 10$, R_f becomes a constant. The present experiments are not designed to find the relationship between R_f and Ri_l so that the change of R_f as Ri_l increases from zero is not determined. However, the decrease of R_f at the end of the decay of the final interface implies a decrease of R_f as Ri_l decreases to zero. Also, as Ri_l becomes zero R_f should

approach zero so that an increase of R_f as Ri_l increases from zero can be inferred. This overall behavior is in agreement with the assumption of Phillips/Posmentier as sketched in Figure 1-1a.

The density flux is uniform throughout the layered interior regardless of the interior density gradient. This phenomenon strongly supports the theory of Posmentier (1977). The density flux generated in the bottom boundary layer goes through the layered interior to the top boundary mixed layer without changing the structure of the interior. This implies that turbulence can transport scalar quantities such as salt, heat, or density further than the characteristic length scale of turbulent eddies without changing the interior structure.

During the decay or merging of interfaces, the density flux becomes a local maximum. After a merging or decay, the density flux decreases and the new or remaining interface is intensified. This indirectly supports the relation that R_f decreases as Ri_o increases.

5.1 Suggestions for Further Studies

The idea of minimum step size was not verified. To test the idea, an experiment started with small scale layers is necessary.

The depth of the tank, H, was a restriction to see the evolution of layers near the stability boundary in two aspects. First, the length scale of step, l_s, increases when U/N_i increases, and l_s becomes comparable to H. Second, the advance of the boundary mixed layers overtakes the interior rapidly, especially for large Re. This also makes it difficult to find the stability boundary. An experiment with a deeper tank will give a more clear stability boundary.

This experiment shows that the scale of the initially formed steps is smaller than that of the well-developed steps. What determines the size of the initial step is unknown, yet.

Turner (1968) shows that R_f decreases slowly as Ri increases, when heat, instead of salt, is used to make the stratification. It would be interesting to investigate the

effect of the molecular diffusivity on the structure of the interior steps.

Appendix 1 Parameters of all the runs

Run Number	H (cm)	U (cm/sec)	D (cm)	Re	$\overline{\rho}$ (g/cm^4)	N_i^2 (sec^{-2})	Number of Cycles	Excursions per Cycle	Cd	Ri
1	41.0	1.0	1.29	129	1.01	0.52	32	250	1.37	0.87
2	41.7	1.7	1.29	223	1.01	0.55	80	100	1.30	0.32
3	41.0	3.0	1.29	387	1.01	0.60	22	50	1.21	0.11
4	41.3	1.0	2.26	226	1.01	0.53	72	100	1.30	2.71
5	41.5	1.7	2.26	390	1.01	0.60	47	50	1.21	1.06
6	41.0	3.0	2.26	678	1.01	0.54	20	30	1.11	0.31
7	41.2	1.0	3.33	333	1.01	0.66	33	50	1.24	7.32
8	41.3	1.5	3.33	496	1.01	0.60	24	30	1.17	2.96
9	40.6	1.6	3.33	390	1.05	2.83	15	100	1.21	12.26
10	40.0	2.8	2.26	626	1.07	3.86	50	100	1.12	2.57
11	40.1	1.7	2.26	391	1.08	4.88	54	150	1.21	8.33
11_1	40.1	1.7	2.26	391	1.08	4.88	80	300	1.21	8.33
12	41.4	2.4	2.26	547	1.01	0.60	20	50	1.16	0.52
13	42.1	2.4	2.26	547	1.02	1.19	50	50	1.16	1.04
14	41.4	2.4	2.26	547	1.00	0.35	20	30	1.16	0.31
15	41.6	2.4	2.26	547	1.03	1.69	75	50	1.16	1.47
16	41.5	2.4	2.26	547	1.02	1.34	65	50	1.16	1.17
17	41.8	2.4	2.26	547	1.05	2.46	57	100	1.16	2.15
18	41.9	2.4	2.26	547	1.07	3.83	83	150	1.16	3.34
19	41.6	2.0	2.26	457	1.04	1.41	42	100	1.17	1.76
20	42.0	2.2	2.26	504	1.03	0.86	50	50	1.17	0.88
21	41.3	2.0	2.26	456	1.02	0.89	50	50	1.17	1.11
23	42.2	2.0	2.26	456	1.02	0.74	49	50	1.17	0.93
24	42.0	2.0	2.26	456	1.01	0.56	45	50	1.17	0.70

Run Number	H (cm)	U (cm/sec)	D (cm)	Re	$\overline{\rho}$ (g/cm^4)	N_i^2 (sec^{-2})	Number of Cycles	Excursions per Cycle	Cd	Ri
26	42.6	1.7	2.26	379	1.00	0.31	37	50	1.23	0.57
27	41.9	2.7	2.26	612	1.00	0.30	15	50	1.13	0.21
28	42.1	1.3	2.26	285	1.00	0.29	45	70	1.27	0.93
29	43.1	2.0	2.26	456	1.01	0.42	50	30	1.17	0.53
30	41.4	2.9	2.26	653	1.01	3.42	120	30	1.12	2.09
31	42.5	2.2	2.26	504	1.00	0.30	30	30	1.17	0.31
32	42.0	2.0	2.26	456	1.00	0.27	30	30	1.17	0.34
33	42.0	2.8	2.26	631	1.03	1.40	65	30	1.12	0.92
34	42.0	2.8	2.26	631	1.04	1.69	70	40	1.12	1.11
35	42.2	2.2	2.26	504	1.00	0.24	20	30	1.17	0.25
36	42.3	2.6	2.26	592	1.03	1.62	60	50	1.13	1.21
37	42.7	2.8	2.26	631	1.02	1.08	50	30	1.12	0.71
38	42.1	3.2	2.26	732	1.03	1.37	50	30	1.08	0.67
39	42.1	1.9	2.26	429	1.00	0.27	35	30	1.19	0.38
40	42.4	3.2	2.26	730	1.02	1.10	40	30	1.08	0.54
41	42.0	2.6	2.26	592	1.02	1.14	38	50	1.13	0.85
42	42.3	3.2	2.26	732	1.02	0.83	35	30	1.08	0.40
43	42.1	2.4	2.26	547	1.02	0.95	40	50	1.16	0.83
44	42.1	4.3	2.26	970	1.01	0.79	32	20	1.00	0.22
45	42.3	3.2	2.26	732	1.05	2.39	55	50	1.08	1.16
46	42.4	4.3	2.26	970	1.02	1.05	28	30	1.00	0.29
47	42.0	4.3	2.26	970	1.05	2.56	24	50	1.00	0.71
48	42.3	3.8	2.26	859	1.02	1.12	35	40	1.11	0.40
50	42.0	4.3	2.26	970	1.03	1.57	35	30	1.00	0.44
51	42.2	1.7	2.26	389	1.00	0.14	21	40	1.21	0.24
52	42.0	4.3	2.26	970	1.08	4.31	30	70	1.00	1.20

Run Number	H (cm)	U (cm/sec)	D (cm)	Re	$\overline{\rho}$ (g/cm^4)	N_i^2 (sec^{-2})	Number of Cycles	Excursions per Cycle	Cd	Ri
53	42.0	4.3	2.26	970	1.04	2.10	22	50	1.00	0.58
54	42.0	3.2	2.26	732	1.07	3.93	45	100	1.08	1.91
55	42.2	3.2	2.26	732	1.05	3.03	45	70	1.08	1.47
56	42.1	4.3	2.26	970	1.06	2.84	35	50	1.00	0.79
57	41.9	3.8	2.26	859	1.06	3.16	35	70	1.11	1.12
58	42.2	3.8	2.26	859	1.07	4.02	30	100	1.11	1.42
59	42.6	3.8	2.26	859	1.03	1.59	18	30	1.11	0.56
60	42.8	3.8	2.26	859	1.05	2.53	40	50	1.11	0.89
61	42.4	3.8	2.26	859	1.04	2.04	40	40	1.11	0.72
62	42.8	2.8	2.26	631	1.01	0.54	30	30	1.12	0.35
63	42.1	5.6	2.26	1254	1.03	1.60	20	25	0.97	0.27
64	42.4	5.6	2.26	1254	1.07	4.10	15	100	0.97	0.68
65	42.3	6.4	2.26	1440	1.03	1.66	25	25	0.96	0.21
66	42.0	6.4	2.26	1440	1.04	2.14	20	40	0.96	0.27
67	42.5	6.4	2.26	1440	1.07	3.89	15	80	0.96	0.49
68	42.1	5.6	2.26	1254	1.04	2.18	22	40	0.97	0.36
69	42.4	6.4	2.26	1440	1.05	2.59	22	40	0.96	0.33
70	42.4	5.6	2.26	1254	1.06	3.14	20	60	0.97	0.52
71	41.9	5.6	2.26	1254	1.05	2.57	20	50	0.97	0.43
72	42.2	6.4	2.26	1440	1.05	3.15	18	60	0.96	0.40
73	42.6	7.1	2.26	1607	1.07	4.11	10	80	0.96	0.42
74	42.3	7.1	2.26	1607	1.05	3.08	16	60	0.96	0.31
75	42.5	2.8	2.26	631	1.01	0.45	22	30	1.12	0.30

Appendix 2 Normalization Constant

Run Number	Constant (erg)	Run Number	Constant (erg)	Run Number	Constant (erg)	Run Number	Constant (erg)
1	6.49E+05	19	1.86E+06	38	1.86E+06	57	4.21E+06
2	7.27E+05	20	1.15E+06	39	3.70E+05	58	5.54E+06
3	7.48E+05	21	1.17E+06	40	1.53E+06	59	2.21E+06
4	6.66E+05	22	1.47E+06	41	1.56E+06	60	3.66E+06
5	7.85E+05	23	9.94E+05	42	1.12E+06	61	2.83E+06
6	7.00E+05	24	7.43E+05	43	1.30E+06	62	7.29E+05
7	6.48E+05	25	7.42E+05	44	1.06E+06	63	2.22E+06
8	8.37E+05	26	4.24E+05	45	3.48E+06	64	5.54E+06
9	7.72E+05	27	3.91E+05	46	1.46E+06	65	2.31E+06
10	3.55E+06	28	3.79E+05	47	3.47E+06	66	2.89E+06
11	4.64E+06	29	5.86E+05	48	1.50E+06	67	5.30E+06
11_1	6.05E+06	30	4.67E+06	49	1.14E+06	68	2.94E+06
12	7.64E+05	31	4.03E+05	50	2.16E+06	69	3.54E+06
13	1.57E+06	32	3.48E+05	51	1.85E+05	70	4.33E+06
14	4.33E+05	33	1.88E+06	52	5.83E+06	71	3.56E+06
15	2.24E+06	34	2.32E+06	53	2.89E+06	72	4.26E+06
16	1.76E+06	35	3.30E+05	54	5.24E+06	73	5.78E+06
17	3.33E+06	36	2.23E+06	55	4.11E+06	74	4.19E+06
18	5.34E+06	37	1.54E+06	56	4.01E+06	75	6.09E+05

References

Batchelor, G. K., 1967, *An introduction to Fluid Dynamics*, Cambridge University Press, Cambridge, 615pp

Fernando, H. J. S., 1991, Turbulent mixing in stratified fluids, *Annual Reviews of Fluid Mechanics*, 23, pp.455-493

Gregg, M. C. 1991, A study of mixing in the ocean: a brief history, *Oceanography*, 4, pp.39-45

Imberger, J. and G. N. Ivey, 1991, On the nature of turbulence in a stratified fluid. Part II: Application to lakes, *Journal of Physical Oceanography*, 21, pp.659-680

Ivey, G. N. and G. M. Corcos, 1982, Boundary mixing in a stratified fluid, *Journal of Fluid Mechanics*, 121, pp.1-26

Ivey, G. N. and J. Imberger, 1991, On the nature turbulence in a stratified fluid. Part I: The energetics of mixing, *Journal of Physical Oceanography*, 21, pp.650-658

Linden, P. F., 1979, Mixing in stratified fluids, *Geophysical and Astrophysical Fluid Dynamics*, 13, pp.3-23

Linden, P. F., 1980, Mixing across a density interface produced by grid turbulence, *Journal of Fluid Mechanics*, 100(4), pp.691-703

Munk, W. H., 1966, Abyssal Recipes, *Deep Sea Research*, 13, pp.707-730

Osborn, T. R. and C. S. Cox, 1972, Oceanic fine structure, *Geophysical Fluid Dynamics*, 3, pp.321- 345

Phillips, O. M., 1972, Turbulence in a strongly stratified fluid-Is it unstable?, *Deep Sea Research*, 19, pp.79-81

Posmentier, E. S., 1977, The generation of salinity finestructure by vertical diffusion, *Journal of Physical Oceanography*, 7, pp.292-300

Ruddick, B. R., T. J. McDougall and J. S. Turner, 1989, The formation of layers in a uniformaly stirred density gradient, *Deep Sea Research*, 36, pp.597-609

Thorpe, S. A., 1982, On the layers produced by rapid oscillating a vertical grid in a uniformly stratified fluid, *Journal of Fluid Mechanics*, 124, pp.391-409

Turner, J. S. 1968, The influence of molecular diffusivity on turbulent entrainment across a density interface, *Journal of Fluid Mechanics*, 33, pp.639-656

Turner, J. S. 1973, *Buoyancy effects in fluids*, Cambridge University Press, Cambridge, 368pp

Turner, J. S., 1981, Small-scale mixing process, In *Evolution of Physical Oceanography*, ed. B. Warren, C. Wunch, pp.236-258, Cambridge, Mass: MIT Press

Woods, J. D., 1968, Wave-induced shear instability in the summer thermocline, *Journal of Fluid Mechanics*, 32(4), pp.791-800

Yoon, K. and Z. Warhaft, 1990, The evolution of grid turbulence under conditions of stable stratification, *Journal of Fluid Mechanics*, 215, pp.601-638